

UNCLASSIFIED

AD NUMBER
AD467052
NEW LIMITATION CHANGE
TO Approved for public release, distribution unlimited
FROM Distribution authorized to U.S. Gov't. agencies and their contractors; Administrative/Operational Use; JUN 1965. Other requests shall be referred to U.S. Naval Postgraduate School, Monterey, CA.
AUTHORITY
USNPS ltr, 6 Jan 1966

THIS PAGE IS UNCLASSIFIED

467052

CATALOGED BY: DDG

UNITED STATES NAVAL POSTGRADUATE SCHOOL



DDC
RECEIVED
AUG 3 1965
DDC-IRA E

**HEAT TRANSFER AND FLOW FRICTION CHARACTERISTICS
OF PERFORATED NICKEL PLATE-FIN TYPE
HEAT TRANSFER SURFACES**

**J.M. BANNON
C.H. PIERSALL, Jr.
P.F. PUCCI**

30 JUNE 1965
Technical Report/Research Paper No. 52

NOTICE: When government or other drawings, specifications or other data are used for any purpose other than in connection with a definitely related government procurement operation, the U. S. Government thereby incurs no responsibility, nor any obligation whatsoever; and the fact that the Government may have formulated, furnished, or in any way supplied the said drawings, specifications, or other data is not to be regarded by implication or otherwise as in any manner licensing the holder or any other person or corporation, or conveying any rights or permission to manufacture, use or sell any patented invention that may in any way be related thereto.

UNITED STATES NAVAL POSTGRADUATE SCHOOL
Monterey, California

Rear Admiral E. J. O'Donnell, USN,
Superintendent

Dr. A. E. Vivell,
Academic Dean

ABSTRACT:

Experimental results for the convective heat transfer and flow friction characteristics of plate-fin type heat transfer surfaces are presented for eight surfaces. Six surfaces were fabricated of perforated nickel plate, one perforated nickel fins with solid nickel plate splitters and one of solid nickel plate. The heat transfer data were obtained by the transient technique and includes the effect of longitudinal conduction.

This task was supported by: Bureau of Ships, Code 645

Prepared by: J. M. Bannon
C. H. Piersall, Jr.
P. F. Pucci

Approved by:
R. W. Bell,
Chairman, Department
of Aeronautics

Released by:
C. B. Menneken
Dean of
Research Administration

U. S. Naval Postgraduate School Technical Report No. 52

30 June 1965

UNCLASSIFIED

Table of Contents

	<u>Page</u>
Introduction	1
Description of Surfaces	1
Presentation of Results	3
Experimental Methods	3
Experimental Uncertainties	5
Discussion of Results	7
Conclusions	11
References	12
Figures	
1. Schematic of Test Apparatus	14
2. Photograph of Test Apparatus	15
3. Geometric and Physical Properties of Slotted Perforated Nickel (160/40 TV and 160/40 Q) "Parallel Plate" Matrices	16
4. Geometric and Physical Properties of Round Perforated Nickel (125 M, 125 P, and 50 G) "Parallel Plate" Matrices	17
5. Geometric and Physical Properties of Slotted Perforated Nickel Fin (160/40 TV) with Solid Splitters "Parallel Plate" Matrix	18
6. Geometric and Physical Properties of Solid Nickel, "Parallel Plate" Matrix	19
7. Geometric and Physical Properties of a Slotted Perforated Nickel (160/40 TV) 20° Skew Matrix	20
8. Enlarged Photograph of the 160/40 TV Perforated Nickel Plate	21
9. f and j vs. N_R 160/40 TV "Parallel Plate" Matrix	22
10. f and j vs. N_R 160/40 Q "Parallel Plate" Matrix	23
11. f and j vs. N_R 125 M "Parallel Plate" Matrix	24
12. f and j vs. N_R 125 P "Parallel Plate" Matrix	25

13.	f and j vs. N_R 50 G "Parallel Plate" Matrix	26
14.	f and j vs. N_R 160/40 TV Fin with Solid Nickel Splitters "Parallel Plate" Matrix	27
15.	f and j vs. N_R Solid Nickel "Parallel Plate" Matrix	28
16.	f and j vs. N_R 160/40 TV 20° Skew Matrix	29
17.	Comparison of Slotted Perforated Nickel, 160/40 TV vs. Solid Stainless Steel, 20° Skew Matrices	30
18.	Comparison of Solid Nickel vs. Theoretical Solutions Parallel Plate Matrices	31
19.	Comparison of Slotted Perforated vs. Solid Nickel "Parallel Plate" Matrices	32
20.	Comparison of Round Perforated vs. Solid Nickel "Parallel Plate" Matrices	33
21.	Comparison of Slotted Perforated Fin with Solid Nickel "Parallel Plate" Matrices	34
22.	Comparison of Slotted Perforated Nickel "Parallel Plate: vs. Slotted Perforated Nickel 20° Skew Matrix	35
23.	Flow Area Goodness Factors for the 160/40 TV Perforated Nickel and the Solid Stainless Steel 20° Skew Matrices	36
24.	Flow Area Goodness Factors for the Slotted Perforated Nickel and the Solid Nickel Parallel Plate Matrices	37
25.	Flow Area Goodness Factors for the Round Perforated Nickel and the Solid Nickel Parallel Plate Matrices	38
26.	Heat Transfer Power vs. Flow Friction Power Per Unit Area for the Slotted Perforated Nickel and Solid Nickel "Parallel Plate" Matrices	39
27.	Heat Transfer Power vs. Flow Friction Power per Unit Area for the Round Perforated Nickel and Solid Nickel and Solid Nickel "Parallel Plate" Matrices	40
28.	Heat Transfer Power vs. Flow Friction Power per Unit Area for the 160/40 TV Perforated Nickel and the Solid Stainless Steel 20° Skew Matrices	41
29.	Enlarged Photograph of the 20° Skew Matrix, 160/40 TV Perforated Nickel	42
30.	Enlarged Photograph of the Modified Parallel Plate Matrix, 160/40 TV Perforated Nickel	42

31. Matrix Holder (Upstream View)	43
32. Matrix Test Section Disassembled (Downstream View)	44
33. Velocity Profile and Temperature Distribution Measurement Device	45
34. Nichrome Wire Heater (Upstream View)	46
35. Close-up of Apparatus Test and Heater Sections	47
36. Recorder Trace of Actual Cooling Curve for 160/40 Q Perforated Nickel, "Parallel Plate" Matrix	48

Tables

I Summary of Heat Transfer and Friction Results - 160/40 TV Perforated Nickel, "Parallel Plate" Matrix	49
II Summary of Heat Transfer and Friction Results - 160/40 Q Perforated Nickel, "Parallel Plate" Matrix	50
III Summary of Heat Transfer and Friction Results - 125 M Perforated Nickel, "Parallel Plate" Matrix	51
IV Summary of Heat Transfer and Friction Results - 125 P Perforated Nickel, "Parallel Plate" Matrix	52
V Summary of Heat Transfer and Friction Results - 50 G Perforated Nickel, "Parallel Plate" Matrix	53
VI Summary of Heat Transfer and Friction Results - 160/40 TV Perforated Nickel Fins with Solid Nickel Splitters, "Parallel Plate" Matrix	54
VII Summary of Heat Transfer and Friction Results - Solid Nickel, "Parallel Plate" Matrix	55
VIII Summary of Heat Transfer and Friction Results - 160/40 TV Perforated Nickel, 20° Skew Matrix	56
C-1 Table of Geometric Properties of Perforated Nickel as Specified by the Manufacturer	

NOMENCLATURE

English Letter Symbols

A	Matrix total heat transfer area, ft ²
A _c	Matrix minimum free flow area, ft ²
A _{fr}	Matrix total frontal area, ft ²
A _s	Solid matrix cross sectional area available for thermal conduction, ft ²
A _k	Conduction area corrected for effect of perforations, ft ²
A*	Plane surface area, ft ²
a	Plate thickness, ft
a	Short side of a rectangular flow passage, ft
b	Plate spacing, ft or in.
b	Long side of a rectangular flow passage, ft
C	Flow stream capacity rate, ($\dot{m}c_p$), Btu/(hr °F)
\bar{C}_s	Matrix capacity, $W_s c_s$, Btu/°F
c _p	Specific heat at constant pressure, Btu/(lbm°F)
c _s	Matrix material specific heat, Btu/(lbm°F)
D _H	Hydraulic diameter, $4r_h$
d	Inside pipe diameter, in.
E	Flow friction power per unit area, HP/ft ²
f	Mean friction factor, dimensionless. This is the "small" or "Fanning" friction factor. (Ratio of wall shear stress to the fluid dynamic head.)
G	Exchanger flow stream mass velocity, (\dot{m}/A_c), lbm/(hr ft ²)
g _c	Proportionality factor in Newton's Second Law, $g_c = 32.2$ (lbm ft)/(lbf sec ²)
h	Unit conductance for thermal convection heat transfer, Btu/(hr ft ² °F), or heat transfer power per unit area per degree temperature difference, Btu/(hr ft ² °F)

English Letter Symbols (continued)

j	Colburn factor = $N_{ST} N_{PR}^{2/3}$, heat transfer characteristic, dimensionless
j'	Colburn j factor based on plane surface area, A^* , dimensionless
K_c, K_e	Contraction loss coefficient for flow at heat exchanger entrance or exit respectively, dimensionless
k	Unit thermal conductivity, $Btu/(hr ft^2 °F/ft)$
k_s	Matrix thermal conductivity, $Btu/(hr ft^2 °F/ft)$
L	Total matrix flow length, ft
\dot{m}	Mass flow rate, lbm/hr
P	Pressure, lbf/ft^2
p	Porosity for matrix surfaces, dimensionless
q	Heat transfer rate, Btu/hr
R	Gas constant, $(ft lbf)/(lbm °R)$, (53.35 for air)
r_h	Hydraulic radius, $(A_c L/A)$, ft, ($4r_h$ = hydraulic diameter)
s	Solidity of a perforated material, $1-u$, dimensionless
T	Absolute temperature, degrees Rankine, °R
t	Temperature, degrees Fahrenheit, °F
V_m	Matrix volume, ft^3
\bar{V}_s	Material volume corrected for effects of perforations
W_s	Mass of matrix, lbm
x	Distance along the flow passage in direction of flow, ft

Greek Letter Symbols

α	Aspect ratio of a rectangular flow passage, b/a , dimensionless
β	Compactness; ratio of total heat transfer area to the volume between the plates, ft^2/ft^3
Δ	Denotes difference
δ	Fin thickness, ft

Greek Letter Symbols (continued)

ζ	Conduction area reduction ratio due to perforations in perforated material; cross sectional area of perforations/cross sectional area, dimensionless
θ	Time
λ	Longitudinal conduction parameter, $\frac{k A_s}{\rho L c_p}$, dimensionless
τ	Time parameter
μ	Fluid viscosity coefficient, lbm/hr ft
ν	Area reduction ratio due to perforations in perforated material, dimensionless
ρ	Density, lbm/ft ³
σ	Ratio of freeflow area to frontal area, A_c/A_{fr} , dimensionless
ϕ	Denotes "function of"
$\bar{\beta}$	Compactness for perforated material including the effect of area reduction, A^*s/V_m , dimensionless
Σ	Summation

Subscripts

atm	Local atmosphere
f	Fluid
i	Initial, individual
k	Equivalent
m	Mean or matrix, as appropriate
o	At orifice
s	(Matrix material) solid
STD	Standard temperature and pressure
1	Upstream
2	Downstream

Dimensionless Groupings

N_R	Reynolds number, $(4r_h G/\mu)$, a flow modulus
$N_{R(p)}$	Reynolds number for pipe, (dG/μ)
N_{St}	Stanton number, (h/Gc_p) , a heat transfer modulus
N_{Nu}	Nusselt number, $(h4r_h/k)$, a heat transfer modulus
N_{Pr}	Prandtl number, $(\mu c_p/k)$, a fluid properties modulus
N_{Tu}	Number of heat transfer units, $(hA/\dot{m}c_p)$
j	Generalized heat transfer grouping - Colburn "j" factor, $(N_{St}N_{Pr}^{2/3})$. This factor versus N_R defines heat transfer characteristics of the surface.
f	Mean friction factor. This is the "small" or "Fanning" friction factor (Ratio of wall shear stress to the fluid dynamic head). This factor versus N_R defines the friction characteristics of the surface.
λ	Conduction parameter, $k_s A_s / \dot{m} L c_p$ for solid material; $k_s A_k / \dot{m} L c_p$ for perforated material
λ_k	Equivalent conduction parameter (corrected for equivalent length in perforated material), λ_k^L
τ	Time parameter, $\frac{hA}{W_s c_s} \theta$

INTRODUCTION

The present investigation is an outgrowth of the continuing program at Stanford University [8]¹ for the evaluation of heat transfer surfaces. The experimental work reported by Howard [4] was performed at the U. S. Naval Postgraduate School, Monterey, and a continuation of that work is presented herein.

DESCRIPTION OF SURFACES

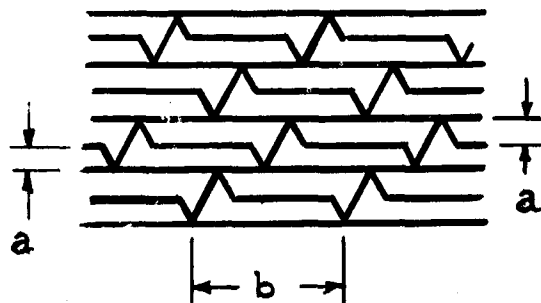
The eight compact heat exchanger surfaces tested were:

1. Skewed passage
 - a. 20° total skew angle; 160/40 TV perforated nickel
2. Modified parallel plate
 - a. 160/40 TV perforated nickel
 - b. 160/40 Q perforated nickel
 - c. 125 M perforated nickel
 - d. 125 P perforated nickel
 - e. 50 G perforated nickel
 - f. 160/40 TV perforated nickel fins with solid nickel splitters
 - g. solid nickel

The skewed passage surface employs corrugated sheets of 160/40 TV perforated nickel, stacked alternately with the lines of corrugations 10° from the flow direction, thereby forming a total angle of 20° between

¹Numbers in brackets refer to numbered items listed in References.

adjacent stacked plates. It is the same geometry as one employed by Howard [4]. The modified parallel plate surfaces were made by alternately stacking a formed plate and a plane splitter plate to prevent nesting, as shown in the sketch below and in the enlarged photograph of Figure 30.



The flow channels formed by this geometry may be compared to rectangular channels with an aspect ratio, $\alpha = b/a$, of about 7.

The perforated nickel plate employed is an electro-deposited metallic sheet of integral structure manufactured by Perforated Products, Incorporated. This material is described in detail in Appendix C. The geometrical and physical properties of the surfaces are given in Figures 3 through 7.

All matrices formed had a frontal cross section of approximately 3.2 inches square and a length of 2.0 inches in the flow direction. All matrices had flow passages with a hydraulic diameter of approximately .002 feet, thus the L/D_H ratio in all cases was of the order of 83.

PRESENTATION OF RESULTS

Heat transfer and flow friction data for each matrix investigated are given in both tabular and graphical form, TABLES I through VIII and Figures 9 through 16, using the Colburn j modulus, Fanning friction factor, and Reynolds number. In evaluating the Reynolds number, the hydraulic diameter, which is defined as four times the hydraulic radius, was used. The effects of entrance, exit, and flow acceleration have been considered in the evaluation of f . (See Appendix A).

Figures 17 through 22 show heat transfer and friction comparisons between various matrices investigated. Also plotted in Figure 18 for comparison purposes are the theoretical laminar flow solutions for parallel plates and rectangular passages [6, 8, 11]. Both solutions are for an infinite length to hydraulic diameter ratio, and the heat transfer solutions are for constant wall temperature. In Figures 23 through 25, "figure of merit" type curves are presented. The j/f versus Reynolds number thus plotted gives an indication of the required matrix flow frontal area for a given pressure drop.

Lastly, in Figures 26 through 28, heat transfer power versus flow friction power curves on a unit area basis, evaluated for fluid properties at standard conditions of dry air at 500°F and one atmosphere, are presented (See Appendix A).

EXPERIMENTAL METHODS

To obtain the heat transfer data, a transient technique was employed. Briefly, this method consists of heating the test matrix by heated air to a uniform temperature (approximately 20°F above ambient in these tests)

and then subjecting the matrix to a step change in the air flow temperature to ambient temperature. The air temperature downstream of the matrix is monitored and recorded versus time. There are several ways of constructing such a test rig [4, 10, 12]. The one used in these tests is shown in Figure 1, and described in detail in Appendix B.

A series of fine nichrome wire heaters were installed upstream of the matrix to heat the air. Turning off the heaters provides the step change in temperature of the air without disturbing the flow. By referencing the thermocouples downstream of the matrix to the thermocouples upstream of the heaters, the initial temperature difference can be very closely controlled. This temperature difference is continuously recorded by a strip chart recorder when a run is made. This recorded trace has the distinct advantage in that there is no transposition of data required which would produce increased uncertainties. Reduction of the data follows the method of Locke [10] and Howard [5], whereby the N_{tu} of the surface can be evaluated by determining the maximum slope of the fluid temperature difference versus time curve during the cooling transient.

Pressure drop data for evaluating the friction factor were obtained from static pressure taps located in the test section immediately upstream and downstream of the matrix. The static pressure immediately upstream of the matrix was also recorded. Velocity profiles were taken just upstream of the matrix to assure that uniform flow conditions were being maintained by the screen pack straightener and by the wire heaters. The flow was measured by an A.S.M.E. standard D and D/2 orifice meter with

changeable orifice plates [14], and was located downstream of the test section. Various manometers were used consistent with the pressure range encountered. All pressure drop data for evaluating the friction factor were taken under ambient air conditions (i.e., isothermal flow). The data reduction relationships are given in detail in Appendix A.

EXPERIMENTAL UNCERTAINTIES

The experimental uncertainties can be considered to be in two categories. First, in the manner in which the experimental gear attempts to meet the idealizations of the experimental method. These are discussed in detail by Howard in [4] and [5].

By insuring uniform flow to the matrix, minimizing the temperature change to minimize fluid property changes, and in the careful design of the fluid heater, these idealizations are met. The second category can be grouped in three areas:

- (1) uncertainty of physical constants,
- (2) inaccuracy in the geometric measurements, and
- (3) instrumentation inaccuracies.

For the determination of the uncertainties reported, the method of Kline and McClintock [9] was used.

(1) Values for the physical constants required were obtained from [1], [2], and [3]. The uncertainties in these values, as best as can be determined, are listed below:

c_s	\pm	0.5%
c_p	\pm	0.5%
N_{Pr}	\pm	2.0%
k_s	\pm	0.5%
μ	\pm	1.0%

It is noteworthy that the accuracy for the value of c_s depends upon the metal used. Where pure metals are used the accuracy quoted is feasible; however, this is not the case with alloys. Thus the tolerance of c_s can be a major cause for inaccuracy [10].

(2) Due to inconsistencies in construction of the matrices, errors in lineal dimensions are considered to be $\pm 0.5\%$. Inasmuch as the weight of the matrix can be determined as accurately as desired, the error in W_s is considered negligible. Based on this, the uncertainties in geometric measurements are considered to be as follows:

$$\begin{aligned} A, A_{fr}, A_c, A_s, A_k, & \pm 1.0\% \\ L & \pm 0.5\% \\ W_s & < 0.1\%, \text{ negligible} \end{aligned}$$

(3) Instrumentation inaccuracies were essentially those obtained in pressure measurement. With the exception of the temperature measurement at the orifice, all temperatures recorded were temperature differences which were recorded in inches (See Appendix A). The temperature measurement at the orifice was obtained by a copper-constantan shielded thermocouple which was read by a Leeds and Northrup portable potentiometer. Assuming adequate manufacturer's calibration of the thermocouple wire, the estimated possible error is \pm one-half of the smallest division on the potentiometer, or ± 0.0025 millivolts which is approximately $\pm 0.1^\circ\text{F}$.

Since the range of pressures varied, requiring several different manometers, the maximum uncertainty encountered was used in the uncertainty analysis. These values are listed below:

$$\begin{aligned} P_o & \pm 1.25\% \\ \Delta P_o & \pm 1.25\% \\ \Delta P_m & \pm 1.70\% \\ P_{atm} & \pm 0.0005'' \text{ Hg (negligible)} \end{aligned}$$

One final parameter for which uncertainty must be determined before an analysis of the experimental results can be made is N_{Tu} . Inasmuch as Colburn j factor is not a linear function of Reynolds number, uncertainty for high and low N_R values was considered. Using Figure 3-A of reference [4] or Figure 5 of reference [5] and the uncertainty in maximum slope as 2.0% the uncertainty interval using reference [9] in the Colburn j factor varies from $\pm 7.5\%$ at high Reynolds Numbers to $\pm 10.2\%$ at low Reynolds Numbers. The uncertainty interval for Reynolds Number is $\pm 2.3\%$, and for the friction factor, f , the uncertainty interval is $\pm 4.3\%$.

DISCUSSION OF RESULTS

The perforated nickel matrices investigated covered a wide range of percent open area, 12 to 50%. Both slotted and round perforated nickel surfaces were evaluated for the "modified parallel plate" geometry. The perforated nickel geometric properties are given in APPENDIX C for the various types investigated. In order to make a reasonable comparison of the performance among these matrices, the same frontal area and flow length were specified. Results are presented in Figures 9 and 10 and listed in TABLES I and II for the slotted perforated nickel matrices; those for the round perforated matrices are given in Figures 11, 12, and 13 and tabulated in TABLES III, IV, and V.

In order to establish a meaningful fiducial point, a solid nickel matrix of the identical material (obtained from the same manufacturer) with the same frontal area and flow length as the perforated matrices was fabricated. The performance of this matrix is illustrated in Figure 15 with tabular values given in TABLE VII.

The best performing slotted perforated nickel matrix was the 160/40Q. The 50G round perforated nickel (50% open area) was the best surface investigated among the "parallel plate" nickel matrices.

As another approach to evaluating the Colburn j factor, j' was considered. The parameter j' is based on the plane surface area, A^* , as if no perforations were present; whereas, j is based on the heat transfer surface area, A , which includes the plate solidity correction, s . The value of j' is readily attainable from the relationship $j' = j \times s$, where $s = A/A^*$. (See Appendix D). The determination of the solidity is fully described in APPENDIX C. Figure 13 for the 50G perforated nickel matrix includes the values for j' versus Reynold's number in addition to the f and j values.

A comparison of the performance of the two slotted perforated matrices together with the solid nickel matrix is shown in Figure 19. A similar comparison for the round perforated nickel matrices is given in Figure 20.

It is readily apparent that the perforated material yields a higher heat transfer characteristic. Inasmuch as the friction factor also shows an increase, a more appropriate comparison can be made from the flow area "goodness" factor curve in Figures 23 through 25. The heat transfer power (h_{STD}) versus flow friction power (E_{STD}) per unit area given in Figures 26 through 28, is another "goodness" factor evaluation. Here the information for each of the matrices is presented based on standard conditions for fluid properties and a common hydraulic diameter. (See APPENDIX A).

So that an appreciation for the perforated material might be realized in direct transfer type of heat exchanger application in addition to its

use in matrix type for rotary regenerators, a "parallel plate" matrix with the 160/40TV perforated nickel fins and solid nickel splitter plates was fabricated. The performance of this matrix is given in graphical and tabular form in Figure 14 and TABLE VI. A comparison with the solid nickel matrix is made in Figure 21. Figure 25 contains the j/f presentation and Figure 26 shows the h_{STD} vs. E_{STD} for this matrix. Here again is a noticeable increase in heat transfer performance, but with a negligible increase in friction factor.

For the 160/40TV perforated nickel material, a 20° skew matrix was compared in performance against the "modified parallel plate" to see how these two configurations compare with one another. The separate performance for each has been mentioned previously; however, the direct comparison is shown in Figure 22. As with the other nickel surfaces, the flow area "goodness" factor is represented in Figure 23.

In the results of this investigation are several items which are general in nature, but nonetheless extremely important. In the laminar Reynolds number range, friction factor is inversely proportional to Reynolds number. By Reynolds analogy, it was anticipated that the Colburn j factor should likewise be inversely proportional to Reynolds number in this region. However, the experimentally obtained values of j in the low laminar Reynolds range utilizing the equivalent conduction length (defined in APPENDIX C) together with Figure 2-A of [4] or Figure 4 of [5] yielded lower than anticipated values for j . Assuming the Reynolds analogy to hold the j vs. N_R experimental curve was extrapolated, shown as a dashed line on the Figures. The j and N_{tu} values obtained in this manner at the given experimental N_R are asterisked in the Tables.

The second item is that of an equivalent conduction length which was stated earlier. In the perforated fin material the slots or round holes, as the case may be, provide for a winding heat flow path. It was appreciated that the matrix flow length, L , was not the true conduction path but somewhat less than actual. A mean conduction path length evaluation is presented in APPENDIX C. The conduction parameter, λ , based on the flow length, L , was evaluated, and by simply multiplying by the ratio L/L_k (also given in APPENDIX C), the value of λ_k was determined.

The entrance and exit length effects for a matrix with a small hydraulic radius are small. In the evaluation for Fanning friction factor (APPENDIX A), the effects of exit and entrance length were considered using values of K_c and K_e from Figures 5-3, -4, or -5 of reference [8], as appropriate. For the perforated surfaces, the K values were taken corresponding to laminar flow conditions.

A final item worth mentioning is again concerned with the low Reynolds range. A slight alteration in the conduction parameter value has a marked effect on the N_{Tu} value in this range. For this reason, when utilizing a nickel material, or any other material with a wide range of specified values for thermal conductivity, it is mandatory that the appropriate value of k_s be obtained. The value of λ is directly proportional to this k_s value, i.e.,

$$\lambda = \frac{k_s A_s}{L m c_p}$$

CONCLUSIONS

A very definite improvement in performance is achieved with the utilization of a perforated material. Kays [6] postulated the improved heat transfer characteristic without "a large amount of form drag so characteristic of high performance surfaces". The perforations apparently disturb the thermal boundary layer to a much greater degree than the hydrodynamic boundary layer. The perforated nickel matrices investigated herein confirm Kays' hypothesis.

The experimentally determined Colburn j values in the low Reynolds range were lower than the j values obtained by extrapolating the j versus N_R curve from the higher Reynolds range. Because of the large uncertainties involved in the low Reynolds range the extrapolated data are considered more reliable.

Effects of longitudinal conduction have been considered in the analysis of data. For the perforated material matrices, corrections for the actual conduction path length and for the area removed by the perforations have been included.

The best performance for a perforated "parallel plate" matrix was attained by the 50G type material.

REFERENCES

1. Eldridge, E. A. and Deem, H. W. Report on Physical Properties of Metals and Alloys from Cryogenic to Elevated Temperatures. Philadelphia: American Society for Testing Materials, 1961.
2. Goldsmith, A., et.al. Handbook of Thermophysical Properties of Solid Materials. Revised Edition, Vol. I, Elements, New York: The MacMillan Company, 1961.
3. Hilsenrath, J., et. al. Tables of Thermodynamic and Transport Properties of Air, Argon, Carbon Monoxide, Hydrogen, Nitrogen, Oxygen, and Steam. New York: Pergamon Press, 1960.
4. Howard, C. P. "Heat Transfer and Flow Friction Characteristics of Skewed Passage and Glass-Ceramic Heat Transfer Surfaces", Technical Report No. 59, Department of Mechanical Engineering, Stanford University, Stanford, California, October 1963.
5. Howard, C. P. "The Single Blow Problem Including the Effects of Longitudinal Conduction", ASME paper No. 64 - GTP - 11.
6. Kays, W. M. "The Heat Transfer and Flow Friction Characteristics of a Wavy Fin, a Strip Fin, and a Perforated Fin Heat Transfer Surface", TR. No. 39, Department of Mechanical Engineering, Stanford University, Stanford, Calif., October 31, 1958.
7. Kays, W. M. and S. H. Clark. "A Summary of Basic Heat Transfer and Flow Friction Design Data for Plain Plate-Fin Heat Exchanger Surfaces", Technical Report No. 17, Dept. of Mechanical Engineering, Stanford University, Stanford, California, August 15, 1953.
8. Kays, W. M. and A. L. London. Compact Heat Exchangers. Second Edition. New York: McGraw-Hill Book Company, Inc., 1964.
9. Kline, S. J. and F. A. McClintock. "Describing Uncertainties in Single-Sample Experiments", Mechanical Engineering, January, 1953, pp 3-8.
10. Locke, G. L. "Heat Transfer and Flow Friction Characteristics of Porous Solids", TR. No. 10, Dept. of Mechanical Engineering, Stanford University, Stanford, Calif., June 1, 1950.
11. London, A. L. "New Developments in Compact Exchangers - Design Theory, Surfaces, and Applications", lecture presented at 6th National ASME - AIChE Heat Transfer Conference, Boston, Massachusetts, August, 1963. Also "Compact Heat Exchangers" in three parts in Mechanical Engineering, Vol. 86, Nos. 5, 6, and 7, 1964.

12. Mondt, J. R. "Effects of Longitudinal Thermal Conduction in the Solid on Apparent Convection Behavior, with Data for Plate-Fin Surfaces", 1961 International Heat Transfer Conference, Boulder, Colorado, Paper No. 73, Proceedings, ASME.
13. Murdock, J. W. "Tables for the Interpolation and Extrapolation of ASME Coefficients for Square-Edged Concentric Orifices", ASME paper, No. 64 - WA/FM - 6.
14. American Society of Mechanical Engineers. Power Test Code Supplements, Instruments and Apparatus, PTC - 19. 5.4 Flow Measurement, Chapter 4. New York: ASME 1959.

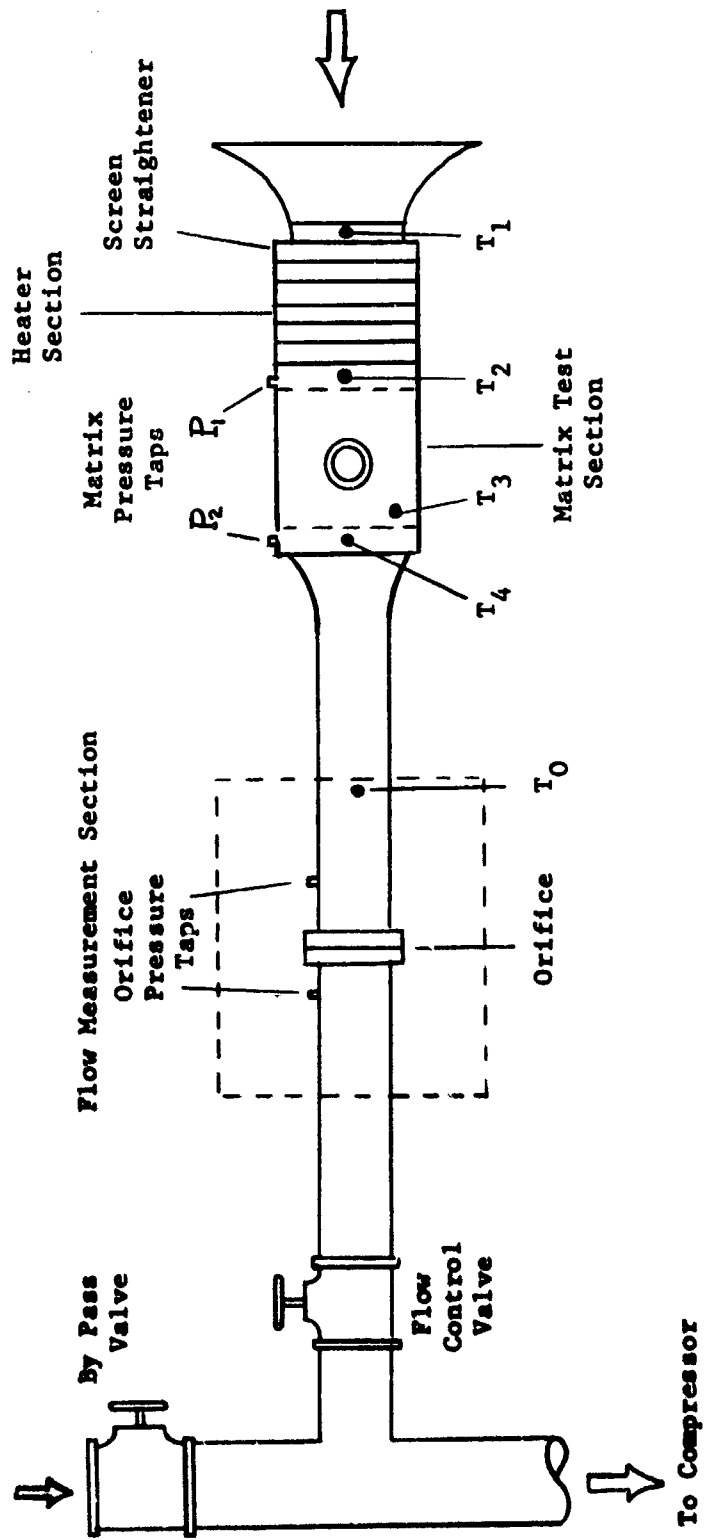
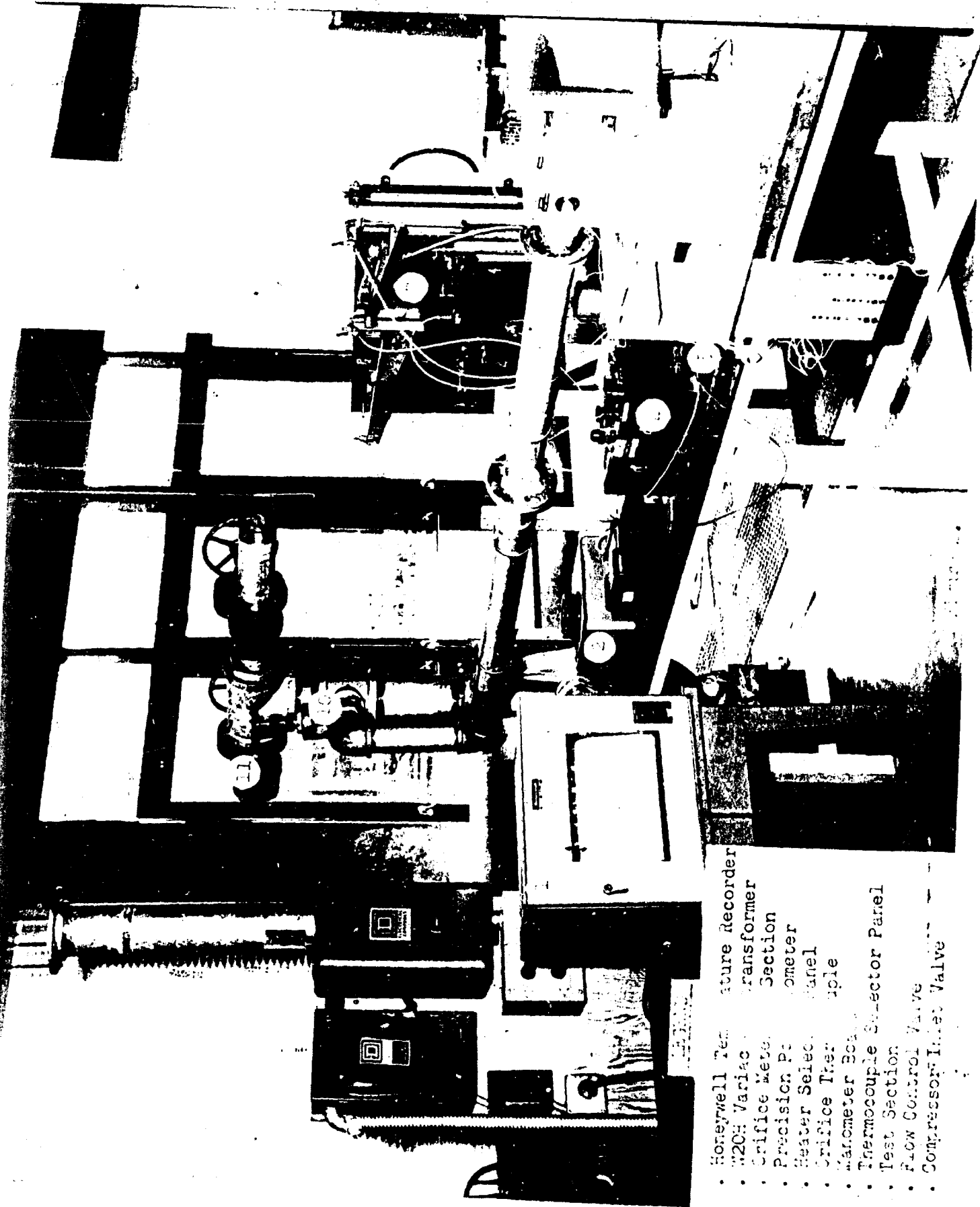
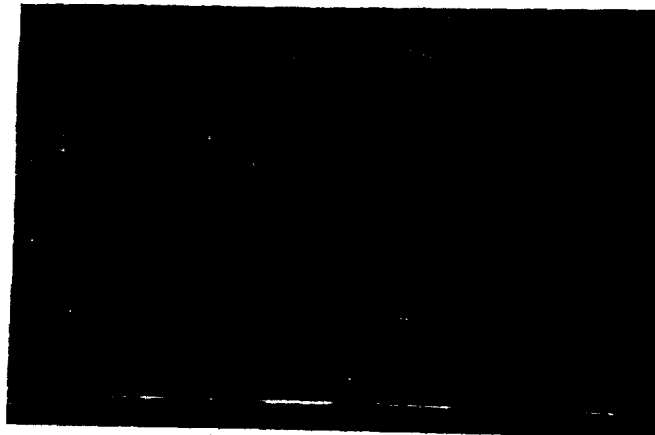


Figure 1. Schematic Diagram of Test Apparatus



- Honeywell Temperature Recorder
- W204 Variac Transformer
- Crifice Meter Section
- Precision Potentiometer
- Heater Selection Panel
- Crifice Thermocouple
- Barometer Back
- Thermocouple Selector Panel
- Test Section
- Flow Control Valve
- Compressor Inlet Valve



2 3 4 5 6 7 8 9 10 11 12 13 14 15 16 17 18 19 20
 3 4

Matrix Material	160/40 TV Perf.Nickel	160/40 Q Perf.Nickel
Specific Heat (c_s) Btu/lb F	0.1065	0.1065
Thermal Conductivity (k_p) Btu/hr ft F	38.7	38.7
Material Thickness, inches	0.0022	0.0016
Total Heat Transfer Area (A) ft ²	18.593	16.2667
Frontal Area (A_{pp}) ft ²	0.06953	0.06953
Total Conduction Area (A_k) ft ²	0.00424	0.002887
Free Flow Area (A_c) ft ²	0.0584	0.06142
Matrix Volume (V_m) ft ³	0.011988	0.011588
Matrix Density (ρ_m) lb/ft ³	53.6	59.2
Hydraulic Diameter (D_H) ft	0.001929	0.002028
Compactness (\bar{Q}) ft ² /ft ³	1604.5	1403.8
Porosity (p)	0.840	0.883

Figure 3. Geometric and Physical Properties of Slotted Perforated Nickel (160/40 TV and 160/40 Q) "Perforated with" Slots

Matrix Material	125 M Perf. Nickel	125 P Perf. Nickel	50 G Perf. Nickel
Specific Heat (c_s) Btu/lb OF	0.1065	0.1065	0.1065
Thermal Conductivity (k_s) Btu/ hr·ft OF	38.7	38.7	38.7
Material Thickness, inches	0.0016	0.0020	0.0016
Total Heat Transfer Area (A) ft ²	16.2578	17.7024	11.2033
Frontal Area (A_{fr}) ft ²	0.06953	0.06953	0.06953
Total Conduction Area (A_k) ft ²	0.00435	0.00640	0.00243
Free Flow Area (A_c) ft ²	0.06142	0.0 5939	0.06142
Matrix Volume (V_m) ft ³	0.011588	0.011588	0.011588
Matrix Density (ρ_m) lb/ft ³	44.1	41.8	31.6
Hydraulic Diameter (D_H) ft	0.002028	0.001961	0.002028
Compactness ($\bar{\epsilon}$) ft ² /ft ³	1403.0	1527.7	966.8
Porosity (p)	0.883	0.854	0.883

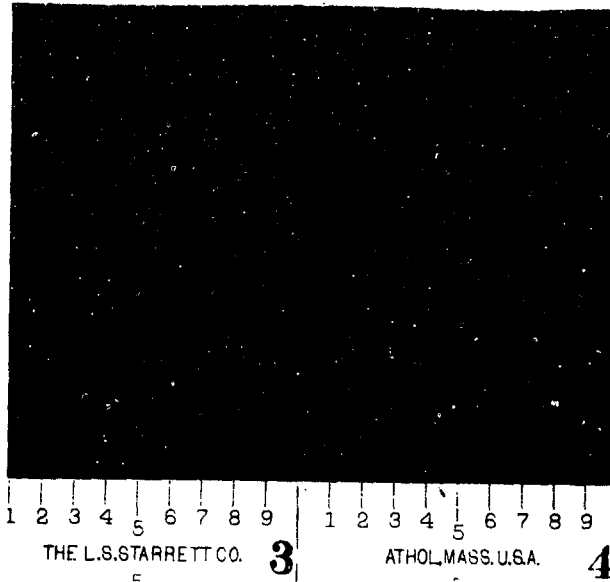
Figure 4. Geometric and Physical Properties of Round Perforated Nickel (125 M, 125 P, and 50 G) "Parallel Plate" Matrices



THE LIBRARY OF THE UNIVERSITY OF MASSACHUSETTS AT LOWELL, U.S.A.

Matrix Material	Solid Nickel
Specific Heat (c_s) Btu/lb °F	0.1065
Thermal Conductivity (k_s) Btu/ hr ft °F	38.7
Material Thickness, inches	0.0020
Total Heat Transfer Area (A) ft ²	20.1875
Frontal Area (A_{fr}) ft ²	0.06953
Total Conduction Area (A_s) ft ²	0.01014
Free Flow Area (A_c) ft ²	0.05939
Matrix Volume (V_m) ft ³	0.011588
Matrix Density (ρ_m) lb/ft ³	77.7
Hydraulic Diameter (D_H) ft	0.001961
Compactness ($\bar{\beta}$) ft ² /ft ³	1742.1
Porosity (p)	0.854

Figure 6. Geometric and Physical Properties of a Solid Nickel "Parallel Plate" Matrix



	20 Degree Skew 160/40 TV Perf. Nickel
Matrix Material	
Specific Heat (c_s) Btu/lb F	0.1065
Thermal Conductivity (k_s) Btu/ hr ft F	38.7
Material Thickness, inches	0.0022
Total Heat Transfer Area (A) ft ²	15.41
Frontal Area (A_{FR}) ft ²	0.0734
Total Conduction Area (A_k) ft ²	0.00349
Free Flow Area (A_c) ft ²	0.06412
Matrix Volume (V_m) ft ³	0.01211
Matrix Density (ρ_m) lb/ft ³	50.1
Hydraulic Diameter (D_H) ft	0.00252
Compactness (\bar{Q}) ft ² /ft ³	1272.8
Porosity (p)	0.873

Figure 7. Geometric and Physical Properties of a Slotted Perforated Nickel (160/40 TV) 20° Skew Matrix

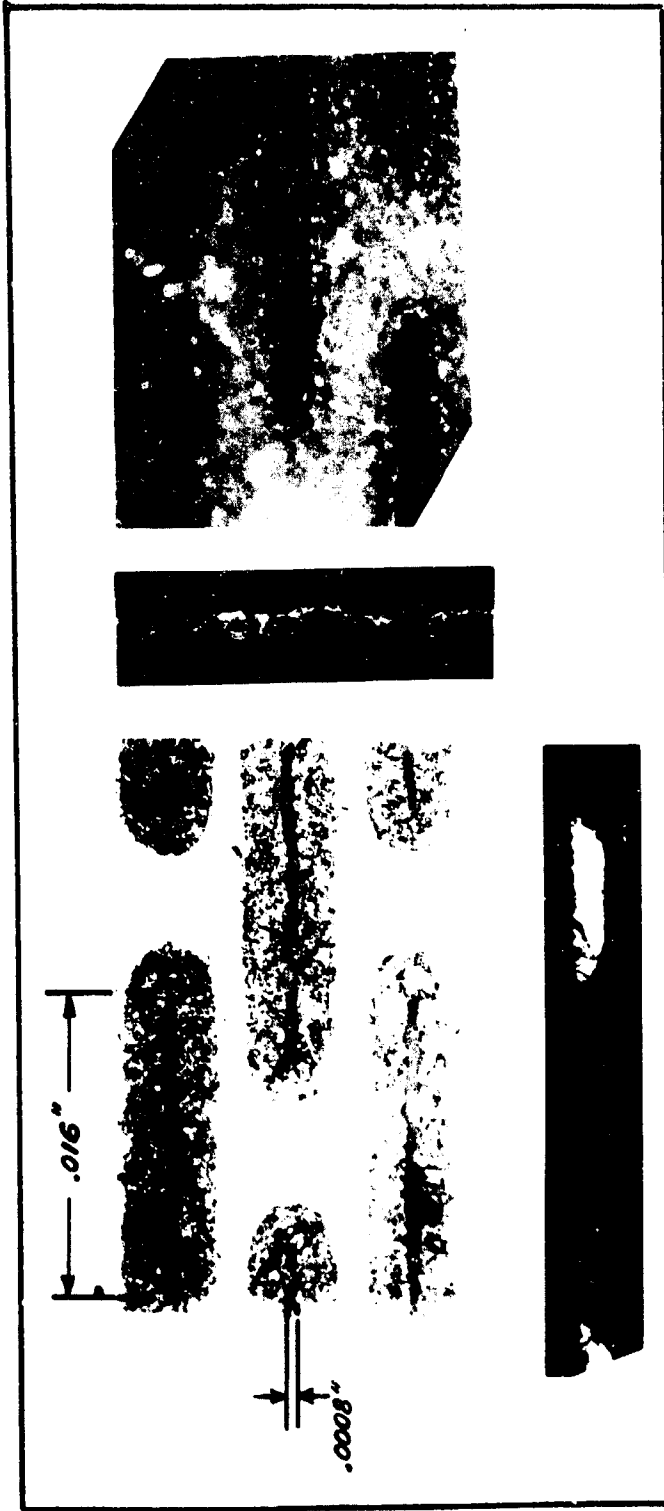


Figure 8. Enlarged Photograph of the 160/40 TV Perforated Nickel Plate

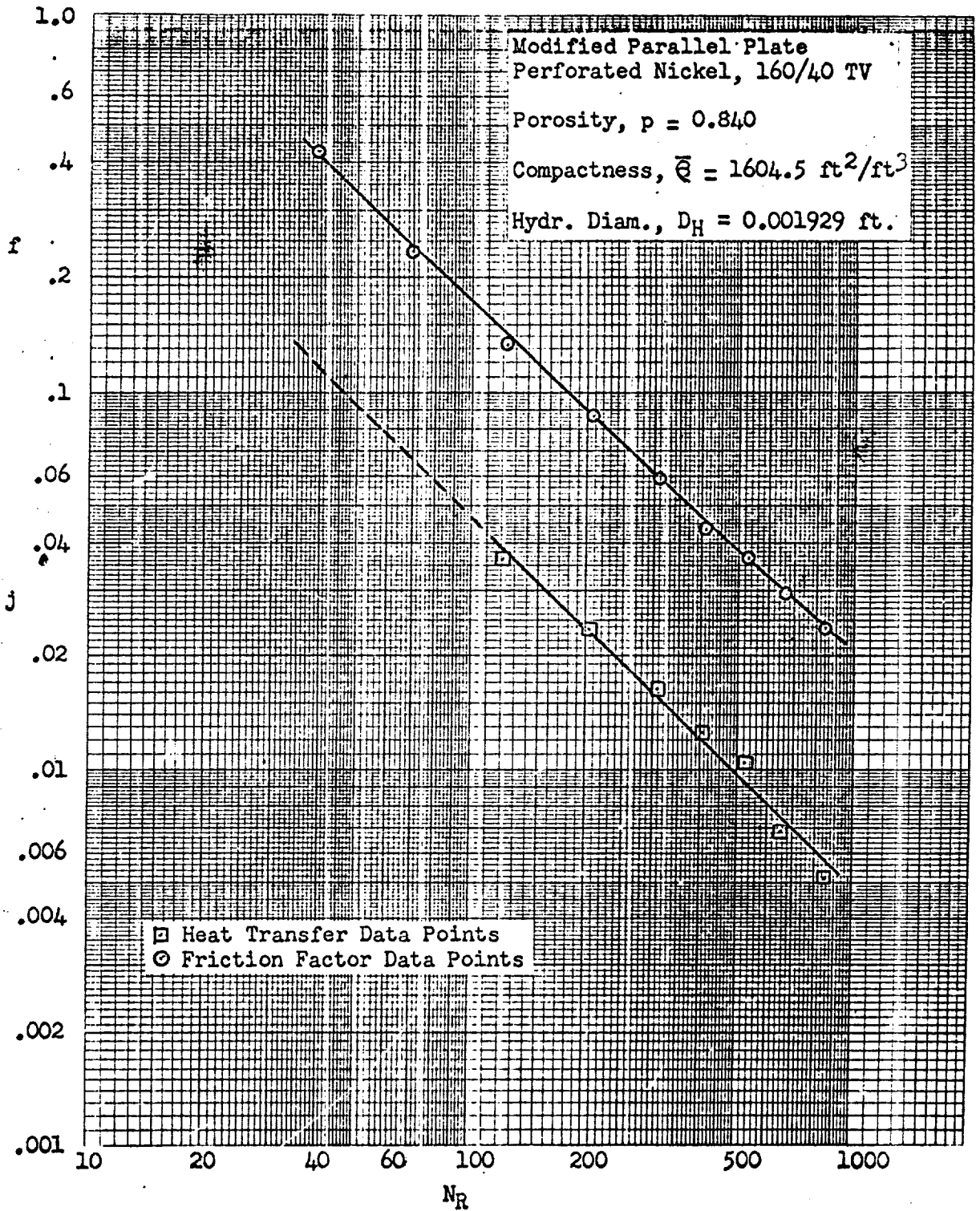


Figure 9. Surface Heat Transfer and Friction Data
 "Parallel Plate", 160/40 TV Perforated Nickel

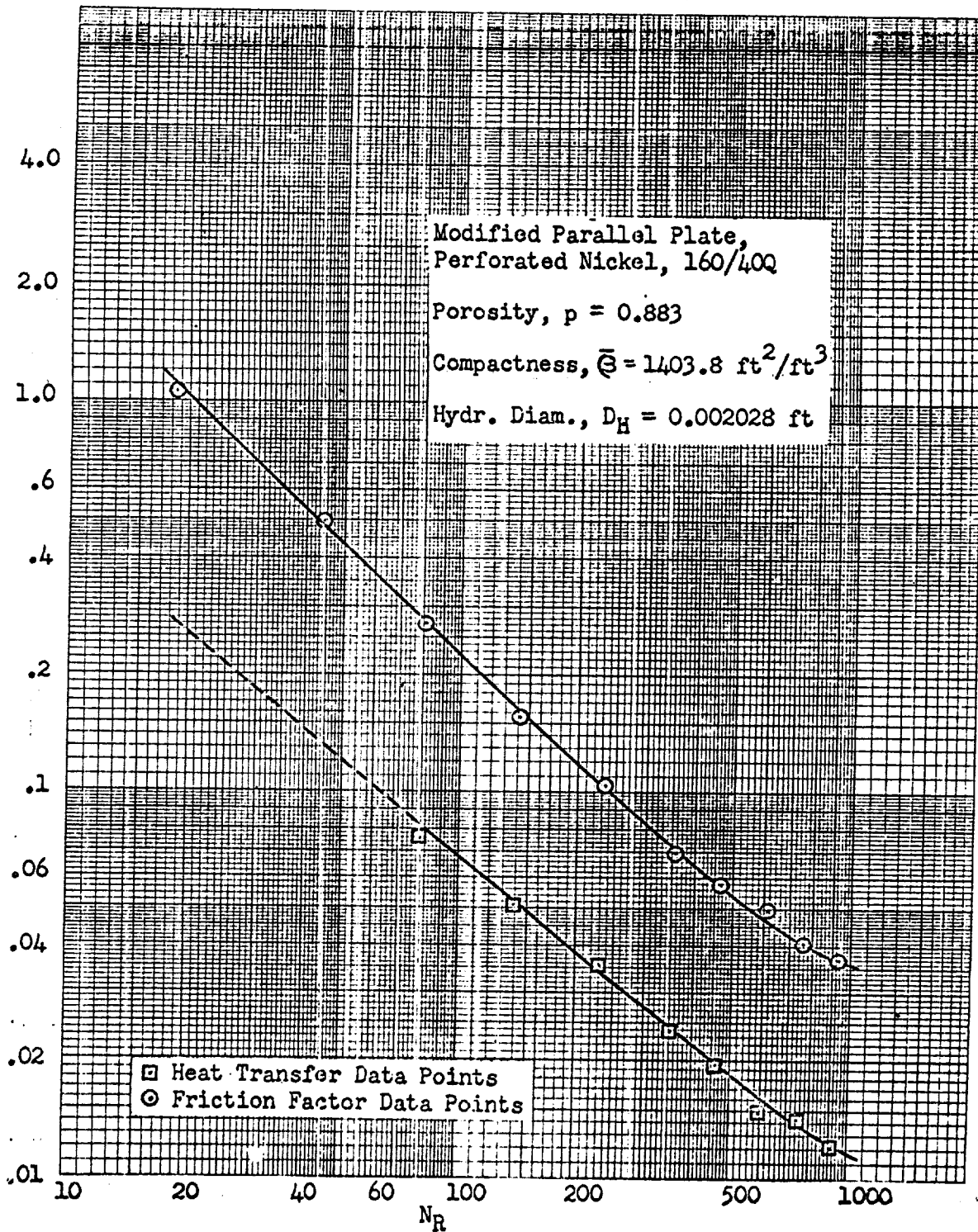


Figure 10. Surface Heat Transfer and Friction Data
"Parallel Plate", 160/40 Q Perforated Nickel

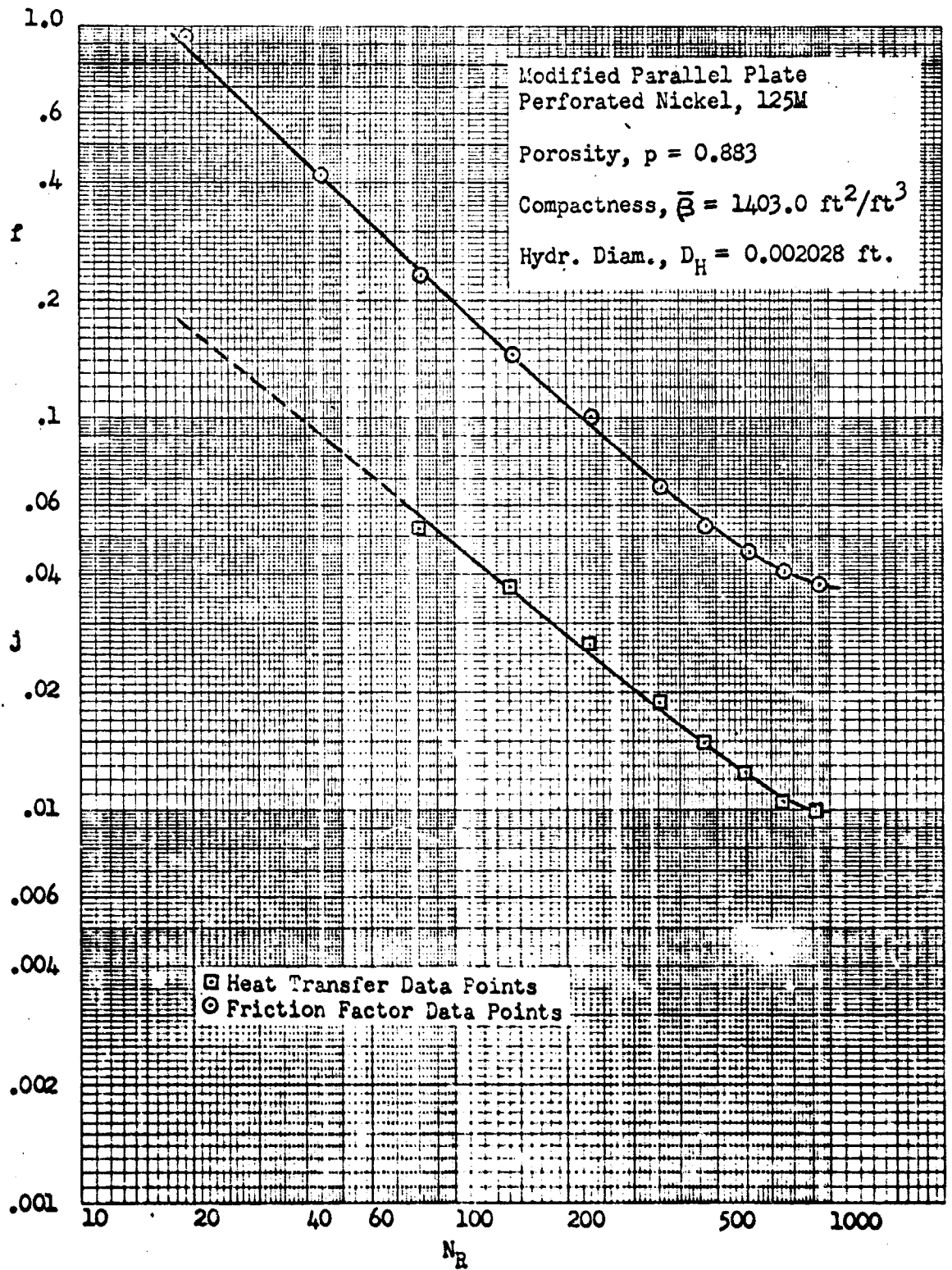


Figure 11. Surface Heat Transfer and Friction Data
 "Parallel Plate", 125 M Perforated Nickel

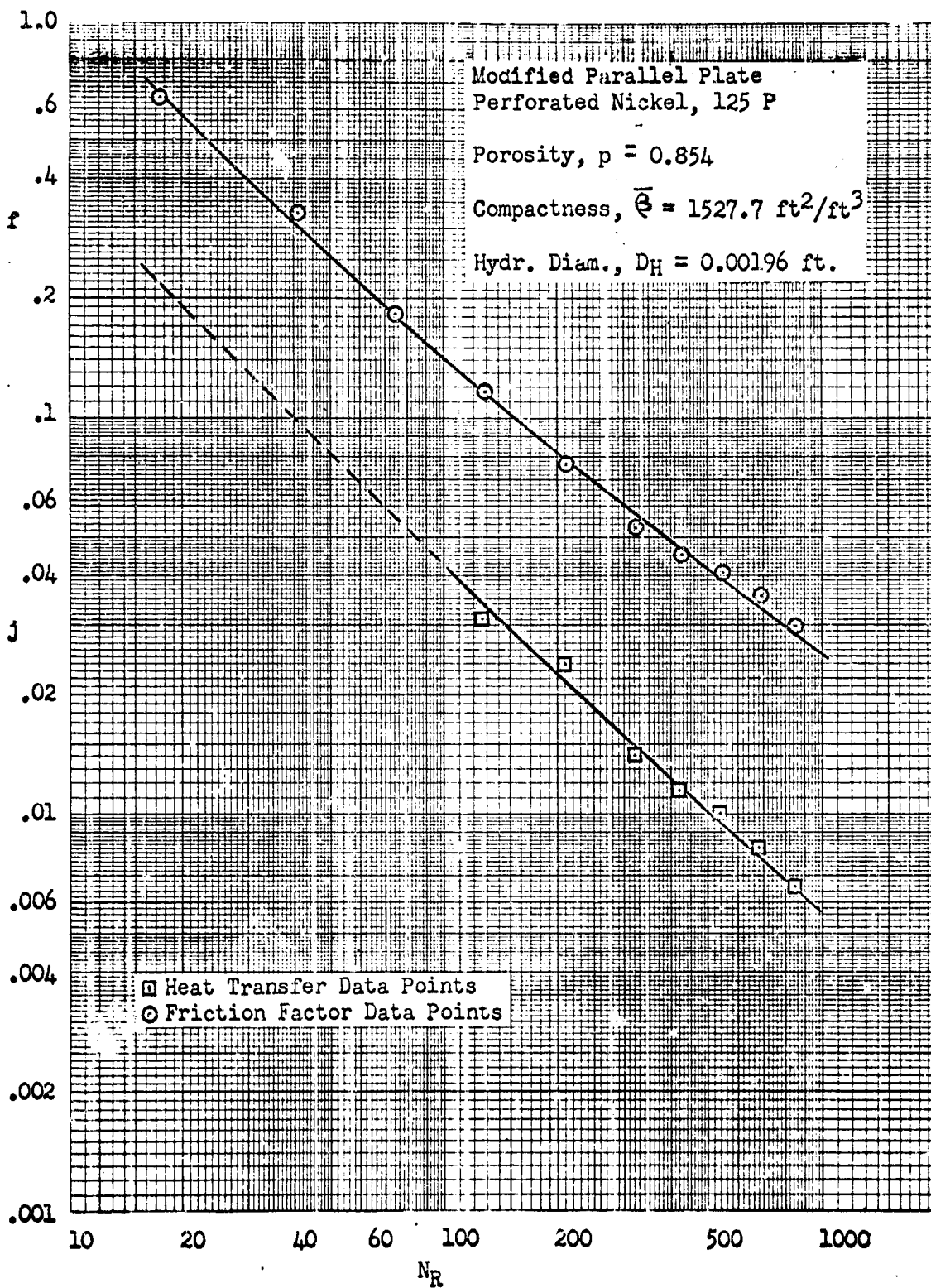


Figure 12. Surface Heat Transfer and Friction Data
 "Parallel Plate", 125 P Perforated Nickel

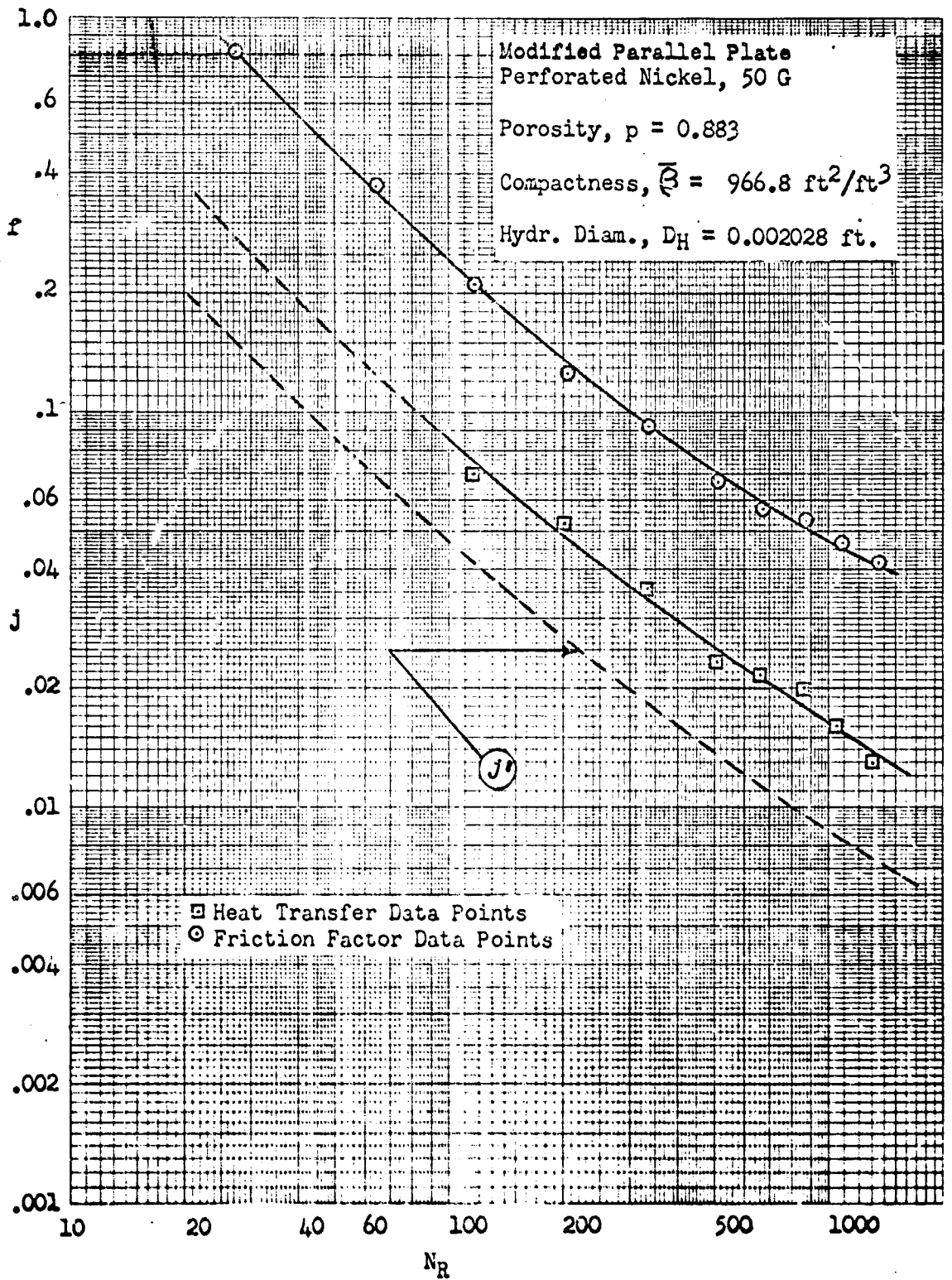


Figure 13. Surface Heat Transfer and Friction Data
"Parallel Plate", 50 G Perforated Nickel

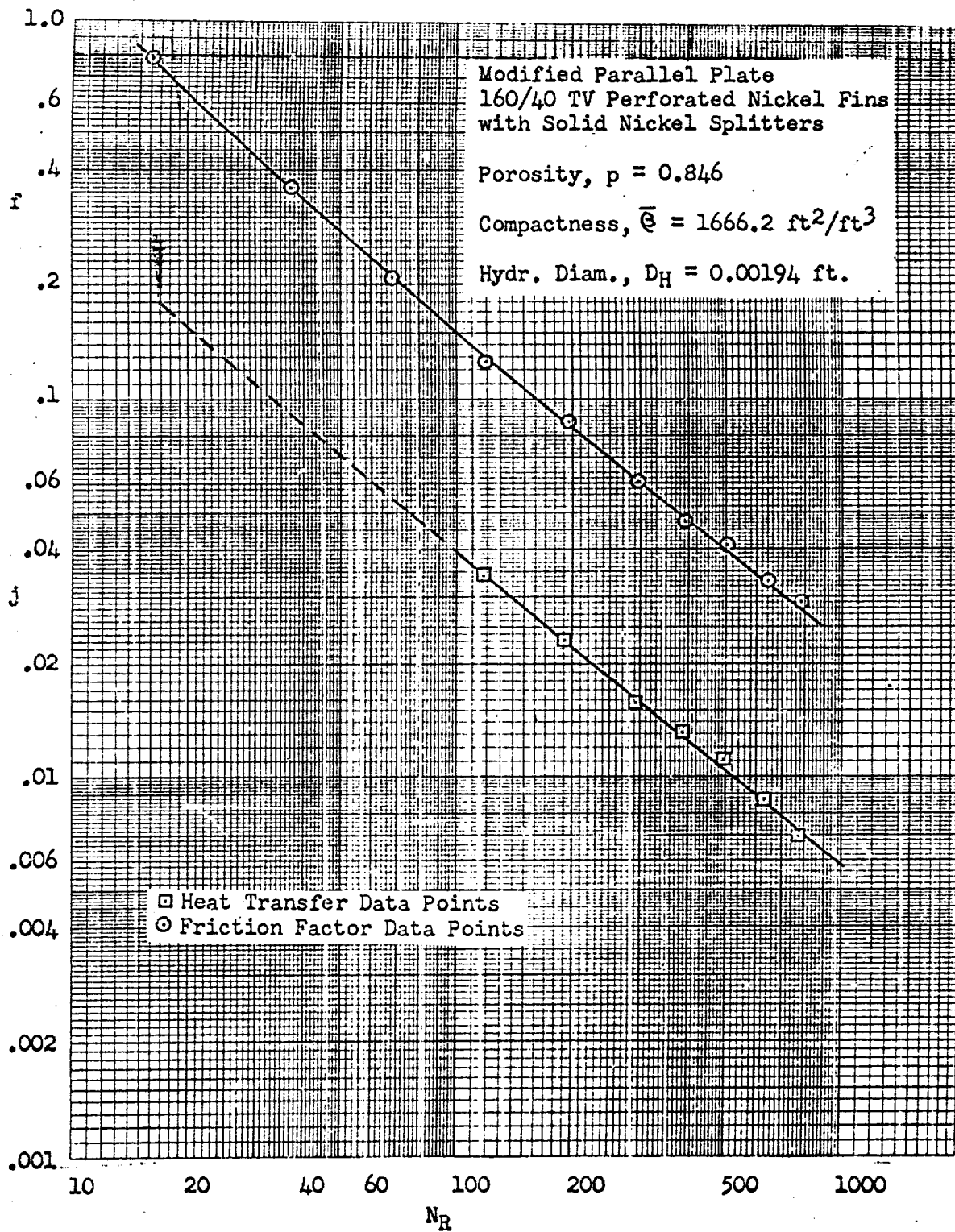


Figure 14. Surface Heat Transfer and Friction Data
 "Parallel Plate", 160/40 TV Fins with Solid
 Nickel Splitter Plates

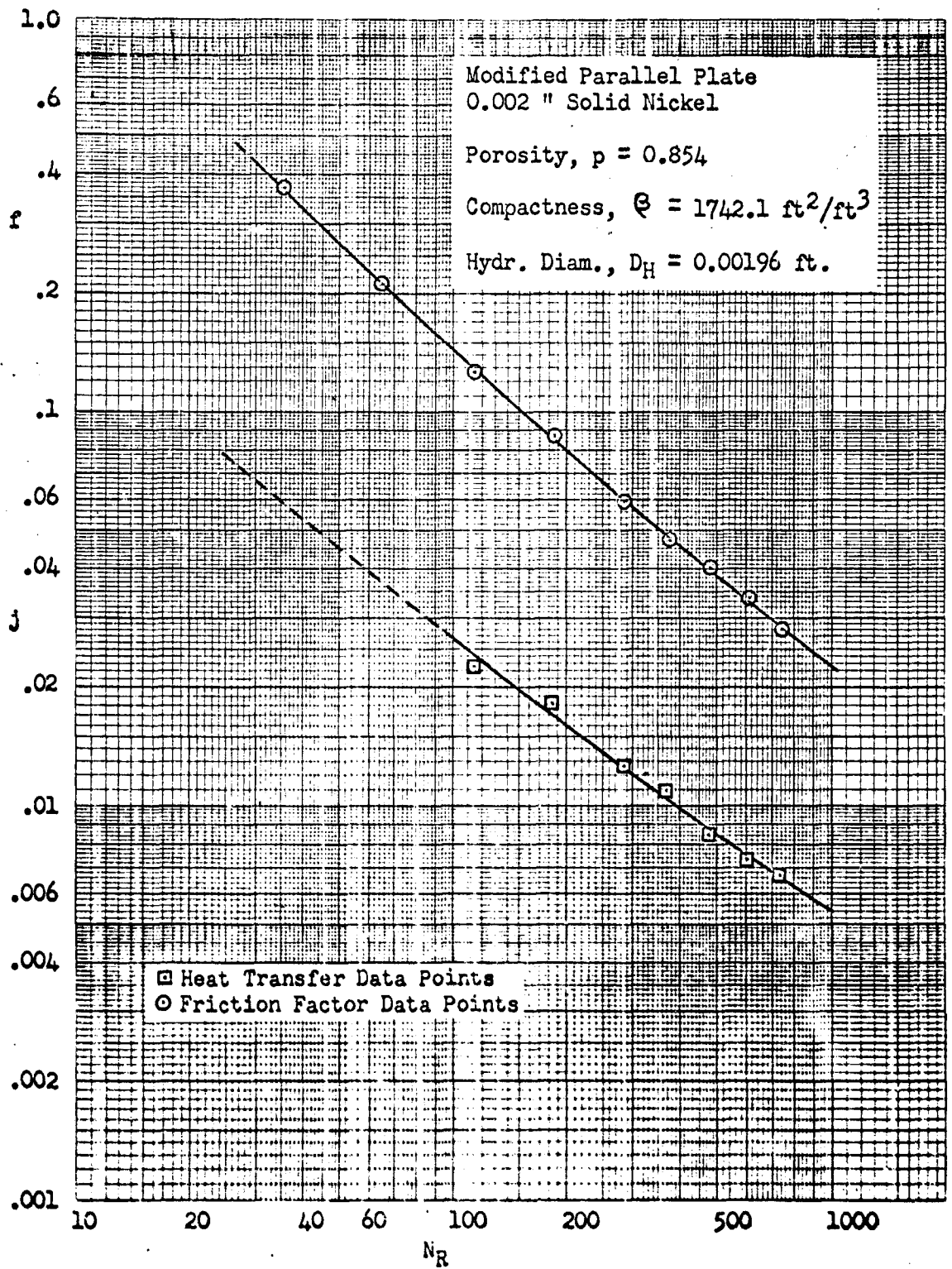


Figure 15. Surface Heat Transfer and Friction Data "Parallel Plate", 0.002" Solid Nickel

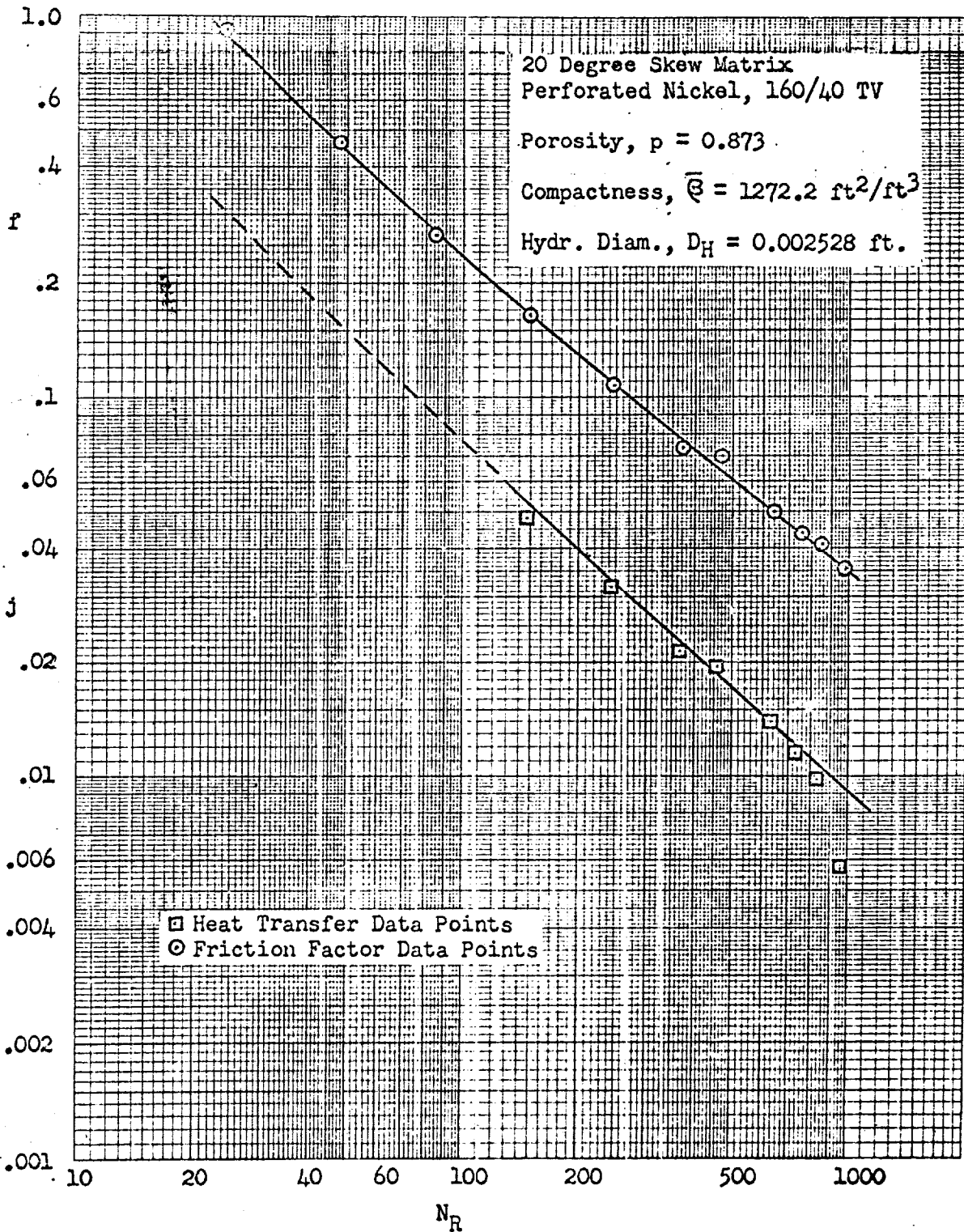


Figure 16. Surface Heat Transfer and Friction Data
20° Skew, 160/40 TV Perforated Nickel

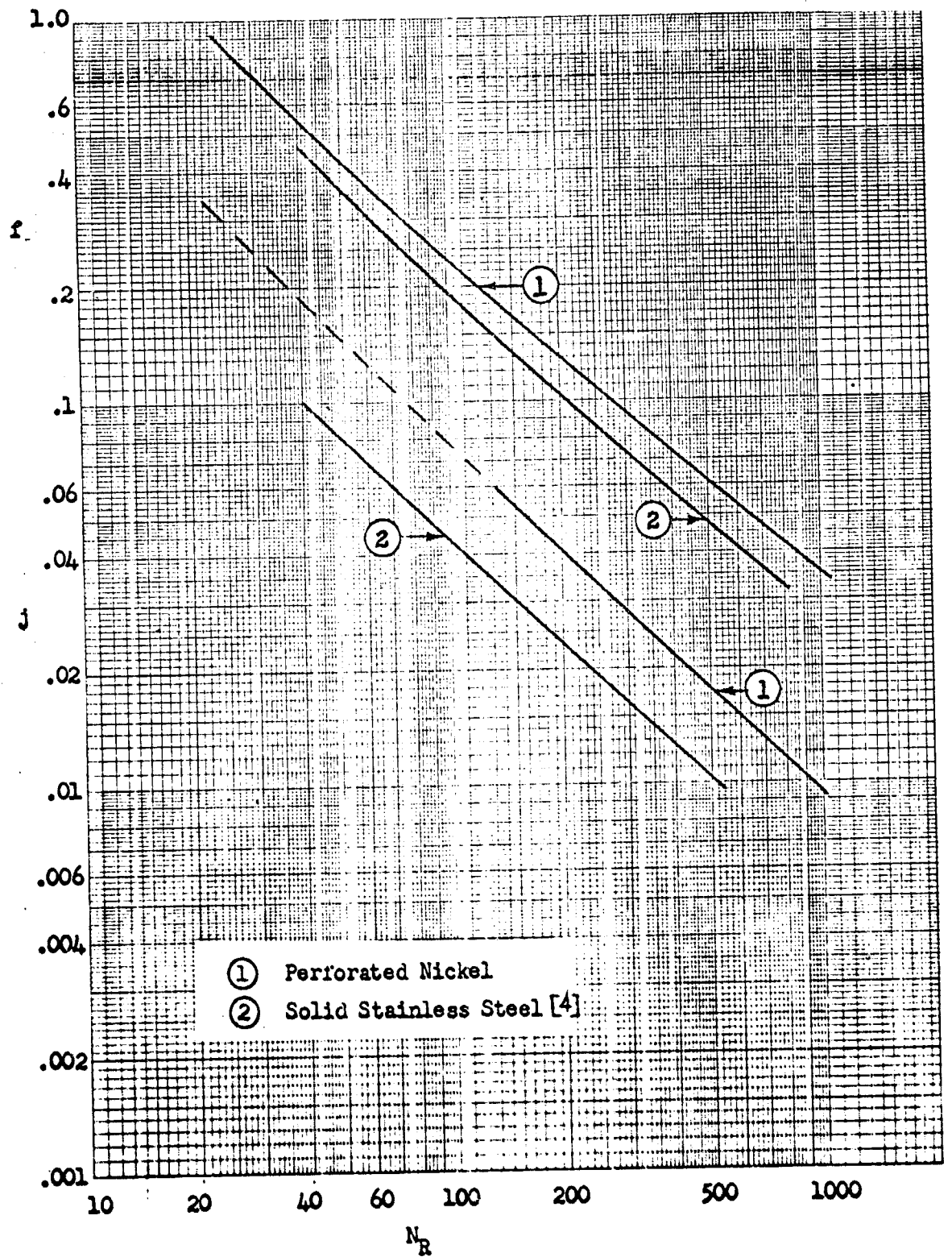


Figure 17. Comparison of Slotted Perforated Nickel, 160/40 TV vs. Solid Stainless Steel, 20° Skew Matrices

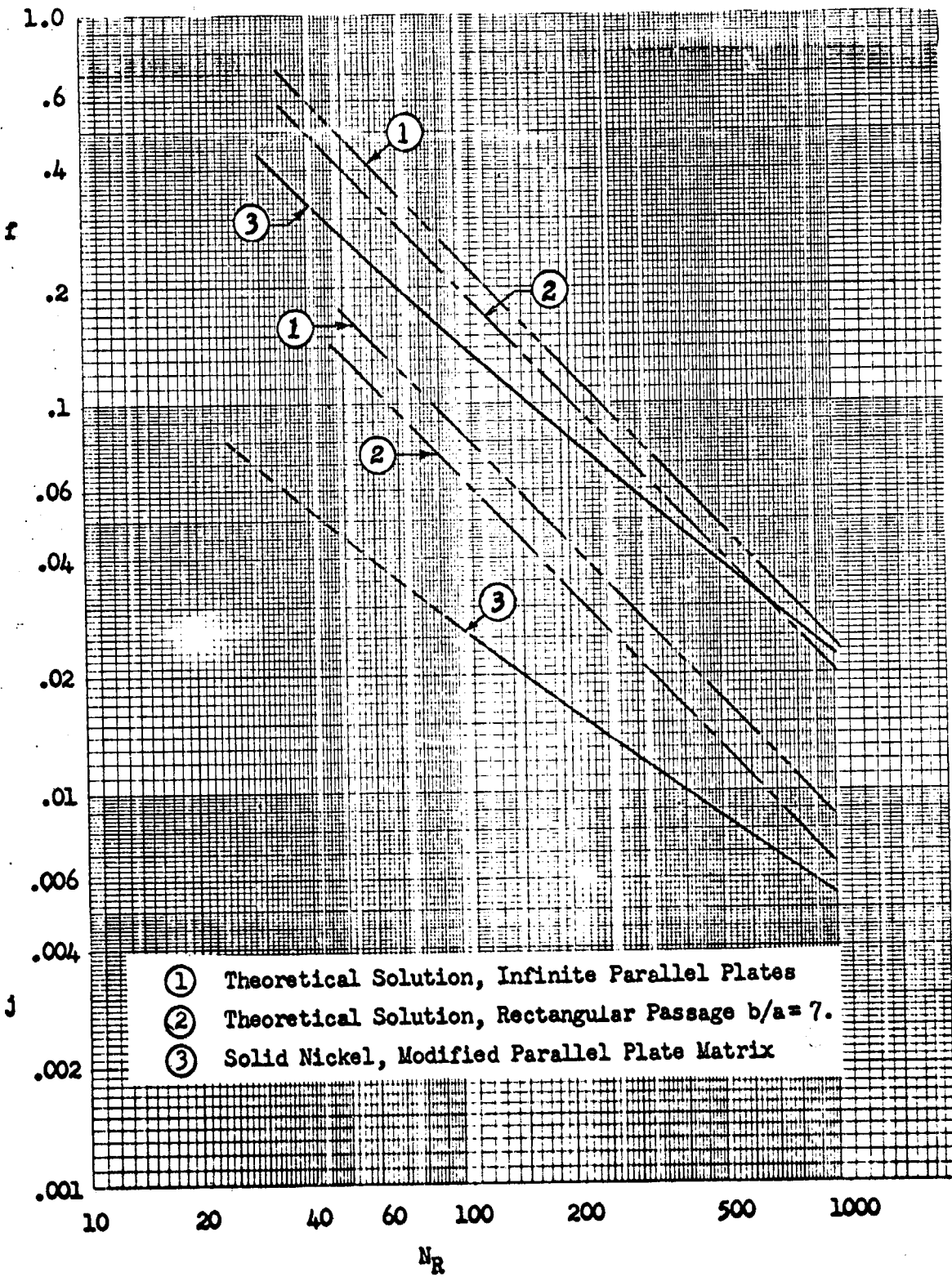


Figure 18. Comparison of Solid Nickel vs. Theoretical Solutions Parallel Plate Matrices

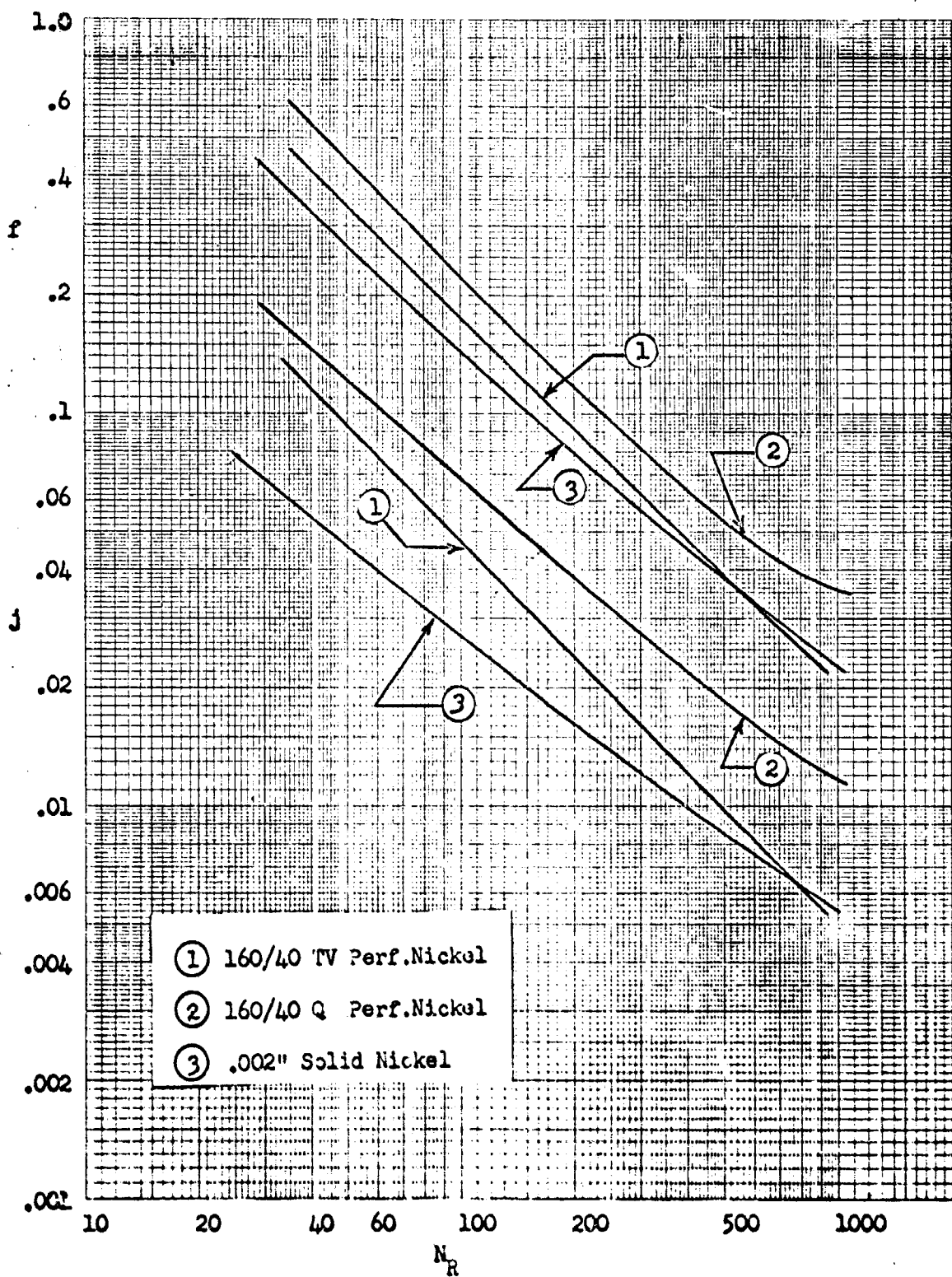


Figure 19. Comparison of Slotted Perforated vs. Solid Nickel "Parallel Plate" Matrices

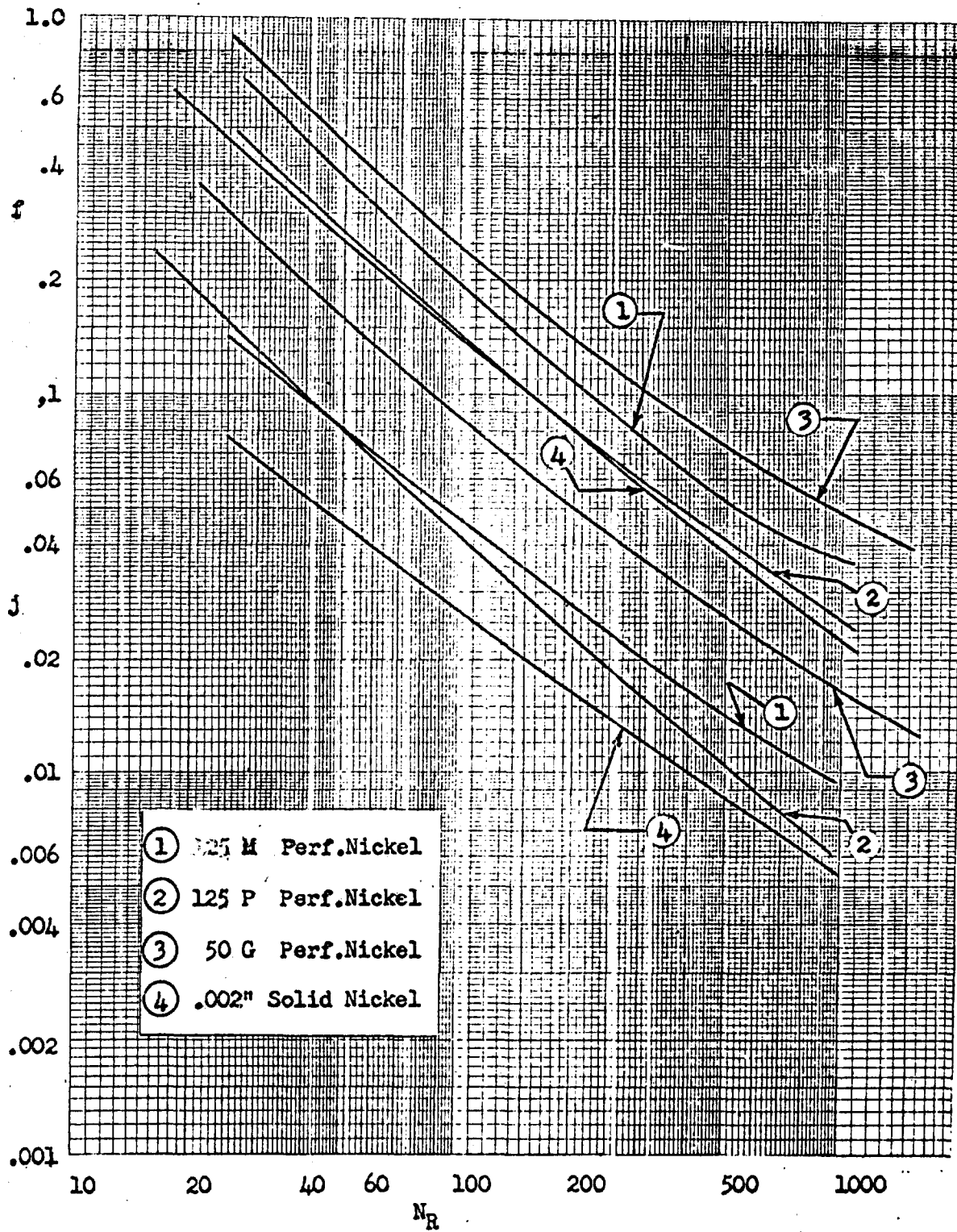


Figure 20. Comparison of Round Perforated vs. Solid Nickel "Parallel Plate" Matrices

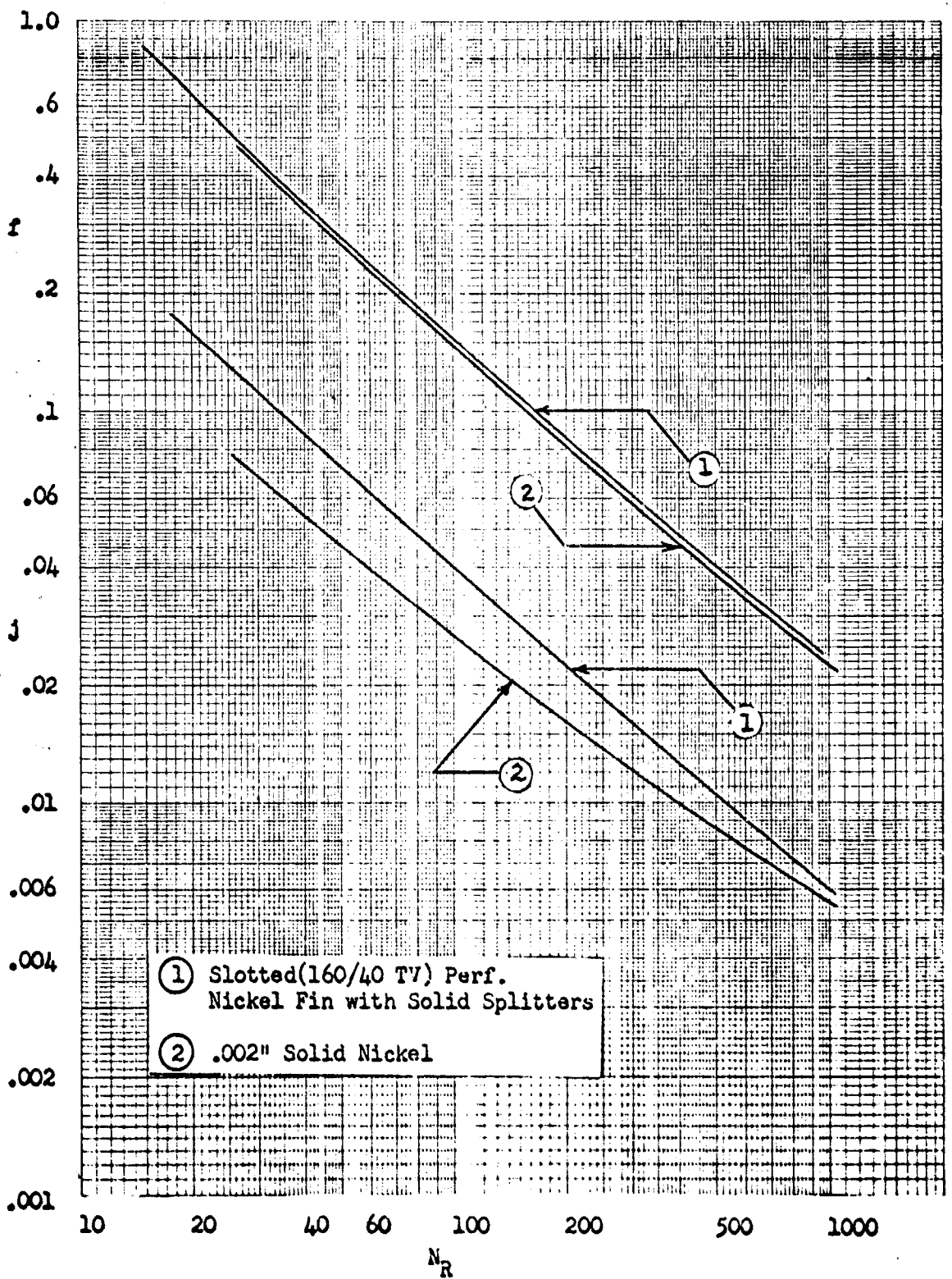


Figure 21. Comparison of Slotted Perforated Fin with Solid Nickel Splitters vs. Solid Nickel "Parallel Plate" Matrices

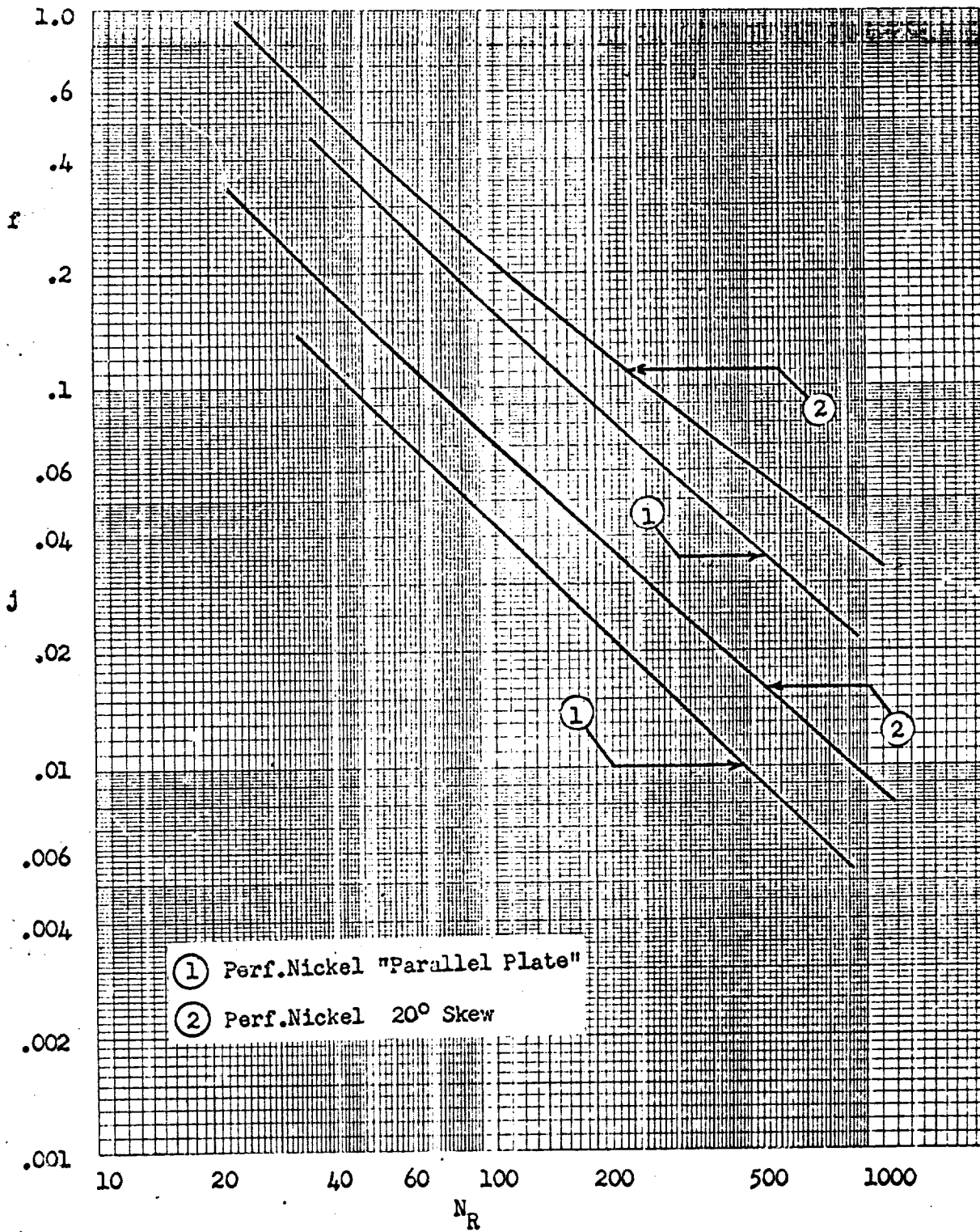


Figure 22. Comparison of Slotted Perforated Nickel "Parallel Plate" vs. Slotted Perforated Nickel 20° Skew Matrix

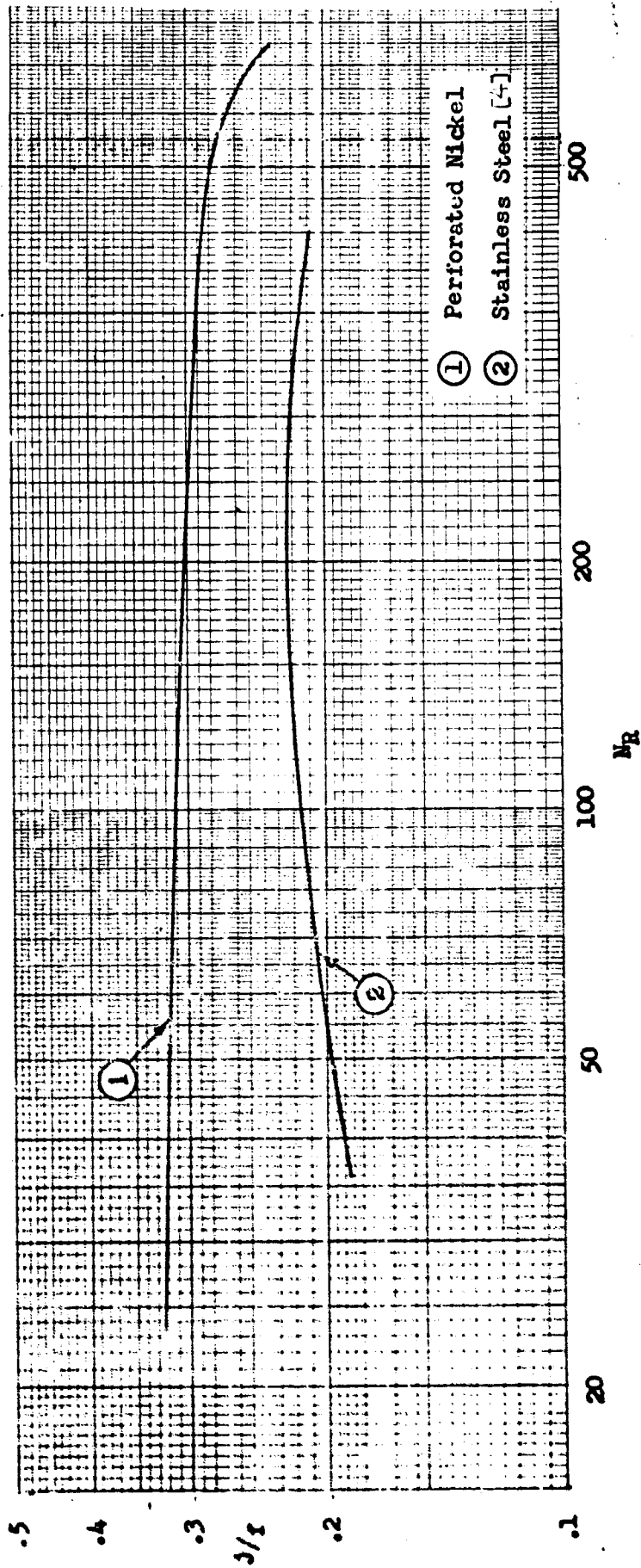


Figure 23. Flow Area Goodness Factors for the 160/40 1V Perforated Nickel and the Solid Stainless Steel 20° Skew Matrices

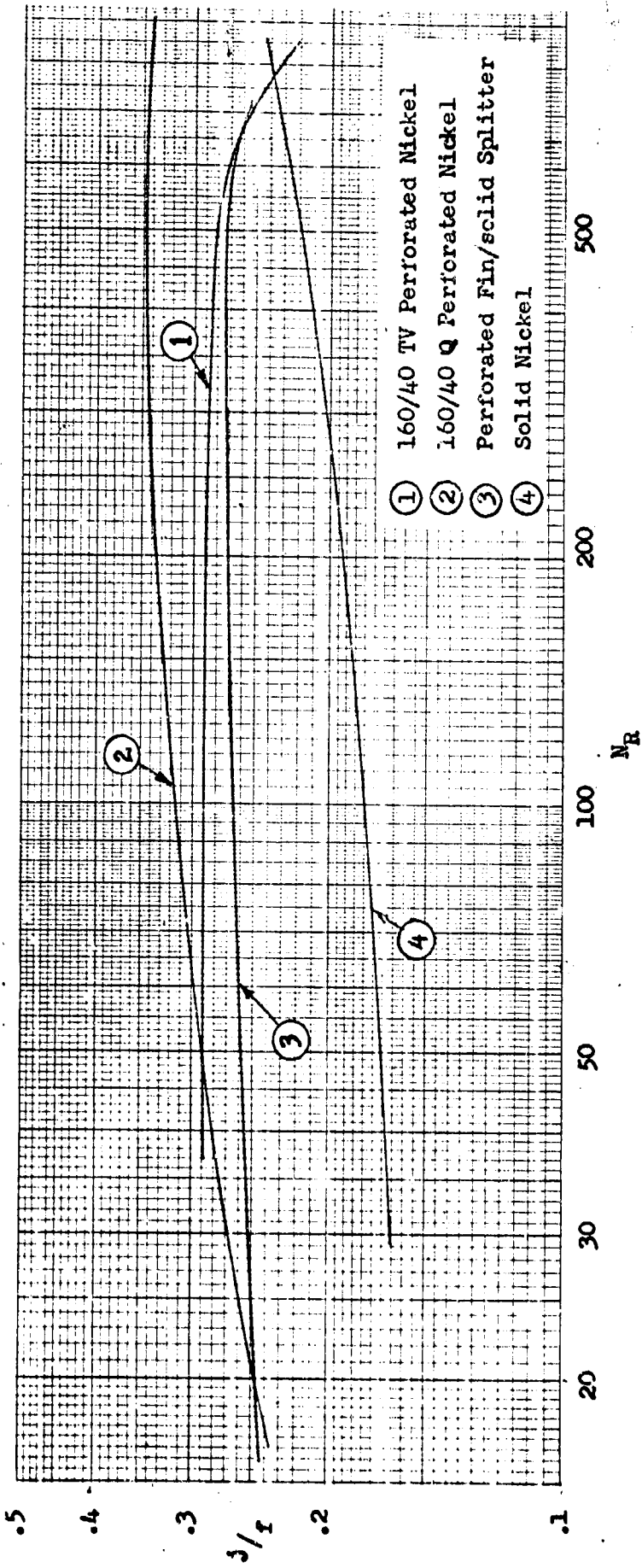


Figure 24. Flow area Goodness Factors for the Slotted Perforated Nickel and the Solid Nickel Parallel Plate Matrices

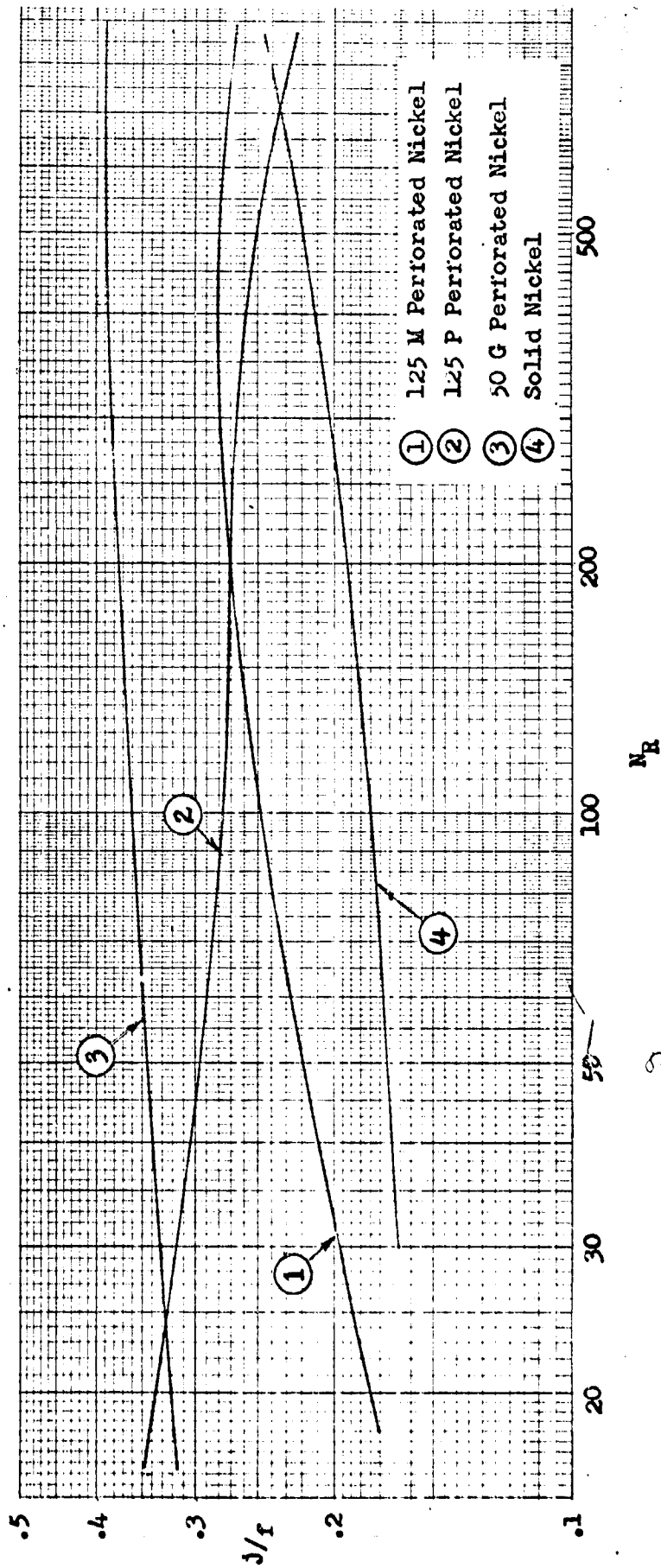


Figure 25. FlowArea Goodness Factors for the Round Perforated Nickel and the Solid Nickel Parallel Plate Matrices

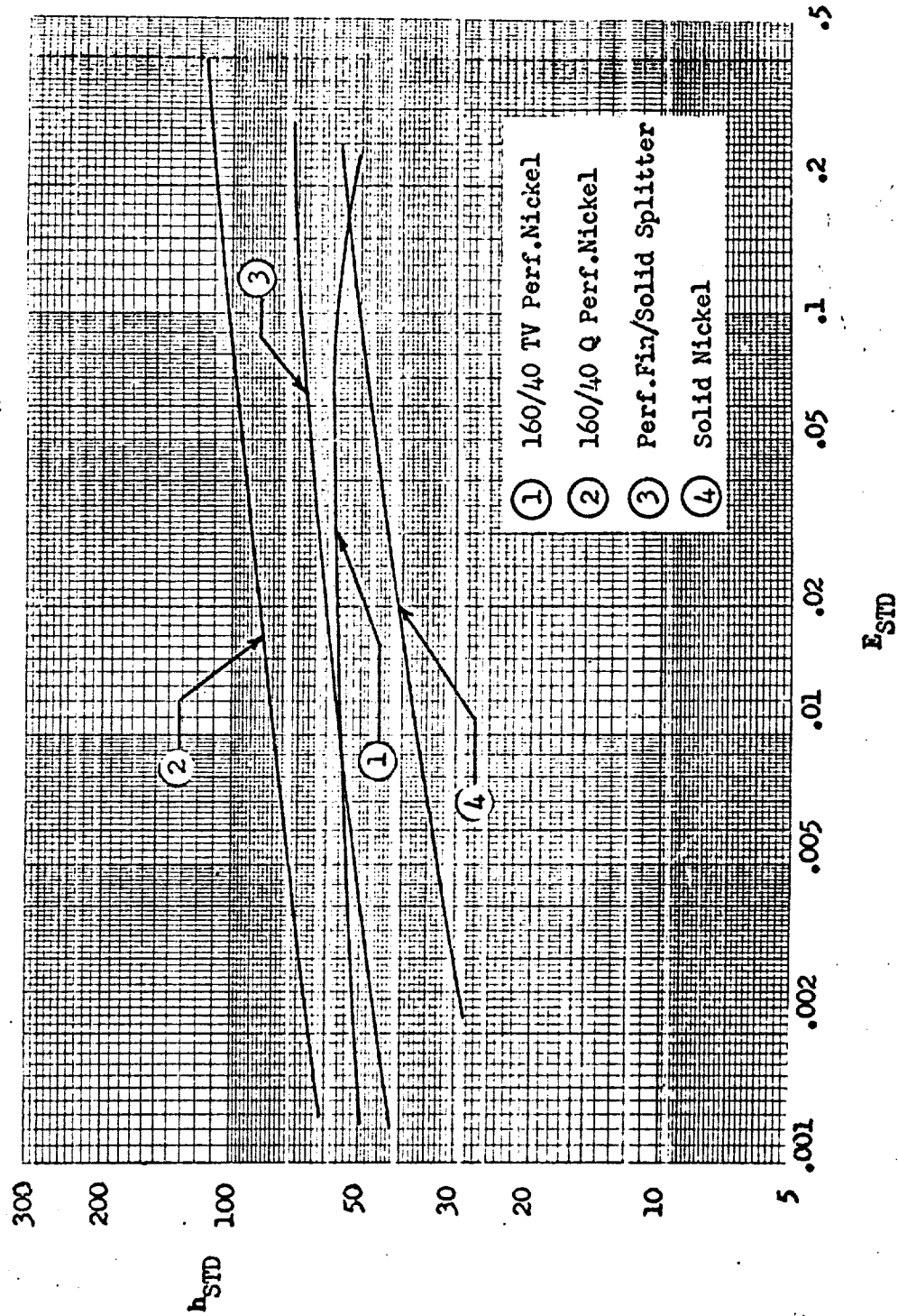


Figure 26. Heat Transfer Power vs. Flow Friction Power per Unit Area for the Slotted Perforated Nickel and Solid Nickel "Parallel Plate" Matrices

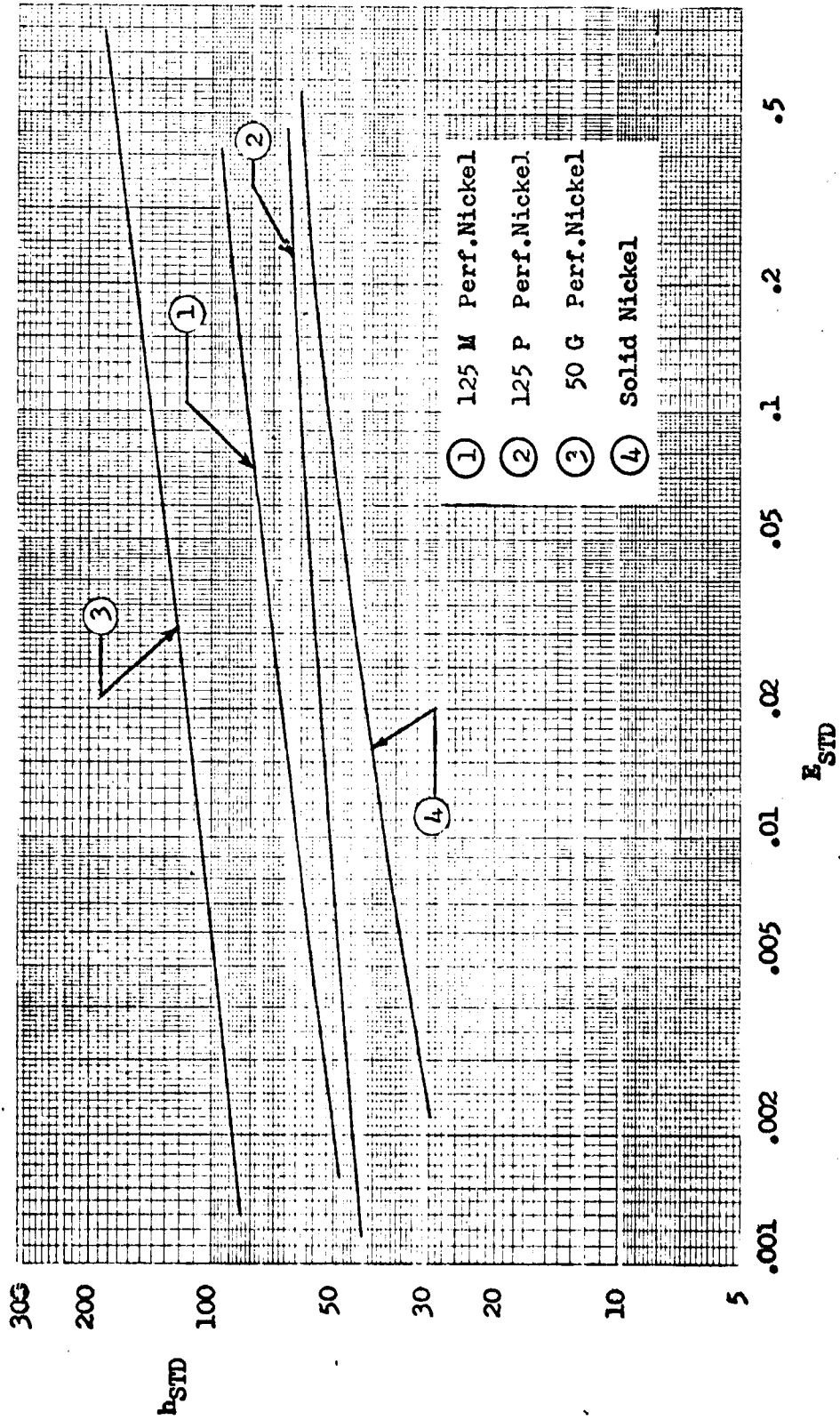


Figure 27. Heat Transfer Power vs. Flow Friction Power per Unit Area for the Round Perforated Nickel and Solid Nickel "Parallel Plate" Matrices

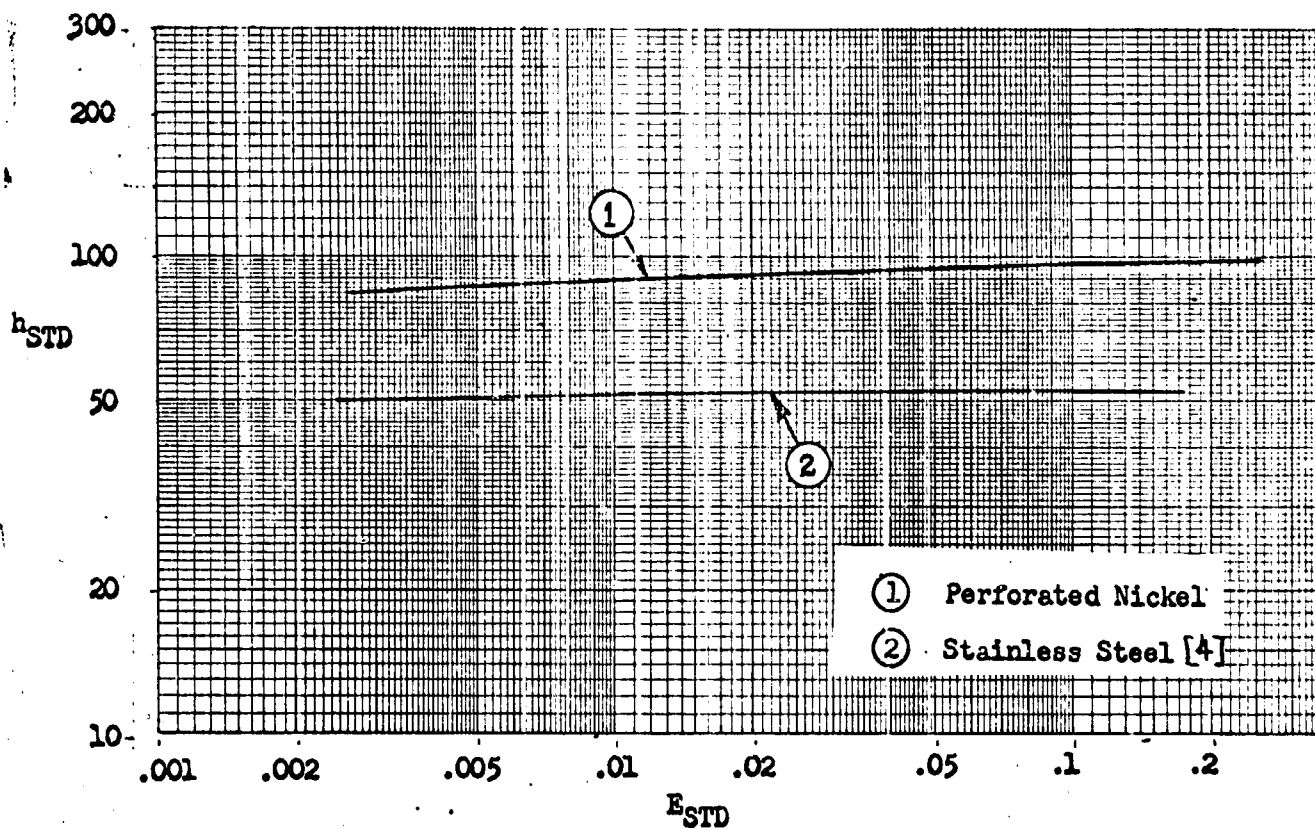


Figure 28. Heat Transfer Power vs. Flow Friction Power per Unit Area for the 160/40 TV Perforated Nickel and the Solid Stainless Steel 20° Skew Matrices

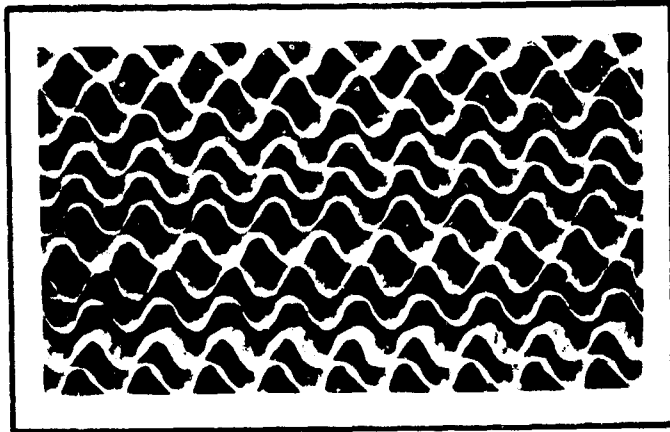


Figure 29. Enlarged Photograph of the 20° Skew Matrix, 160/40 TV Perforated Nickel

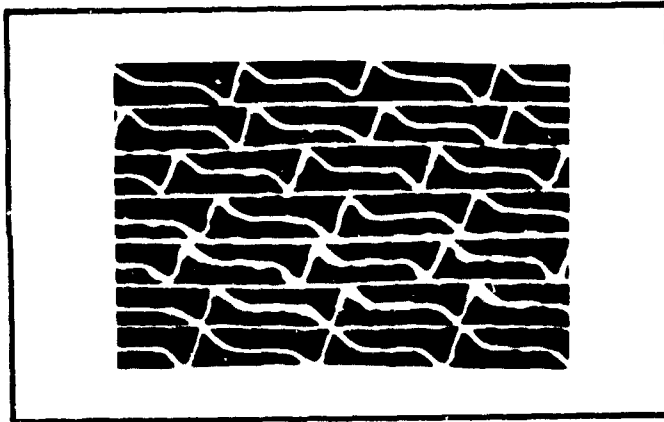


Figure 30. Enlarged Photograph of the Modified Parallel Plate Matrix, 160/40 TV Perforated Nickel

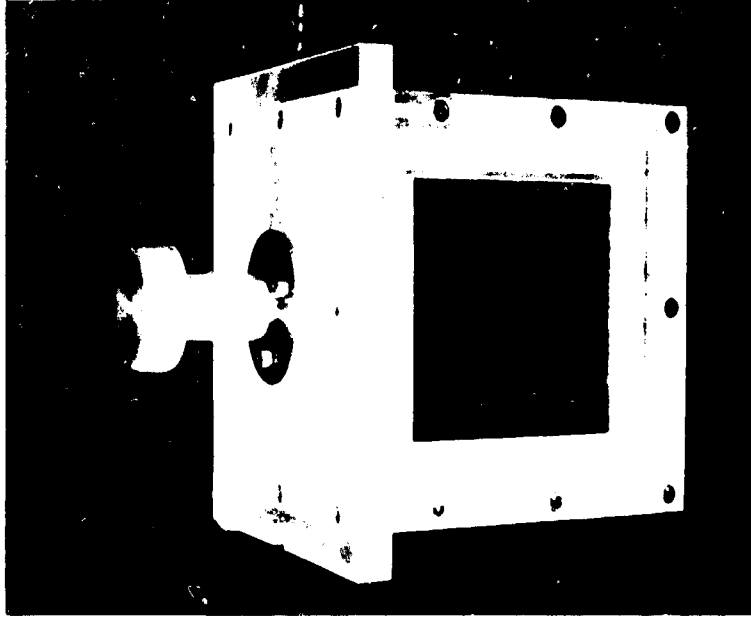
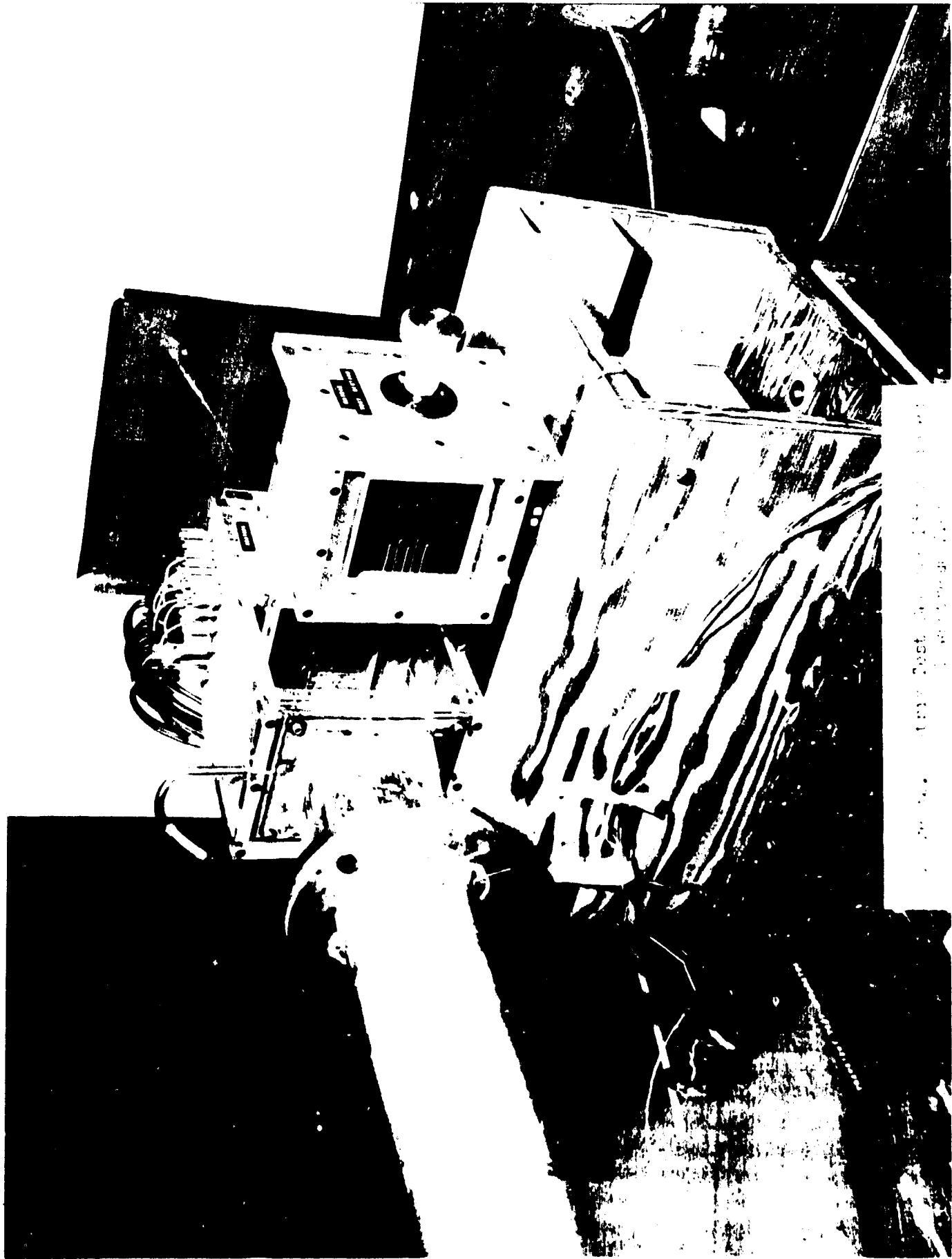


Figure 31. Matrix Holder
(Upstream View)



... the Post ...

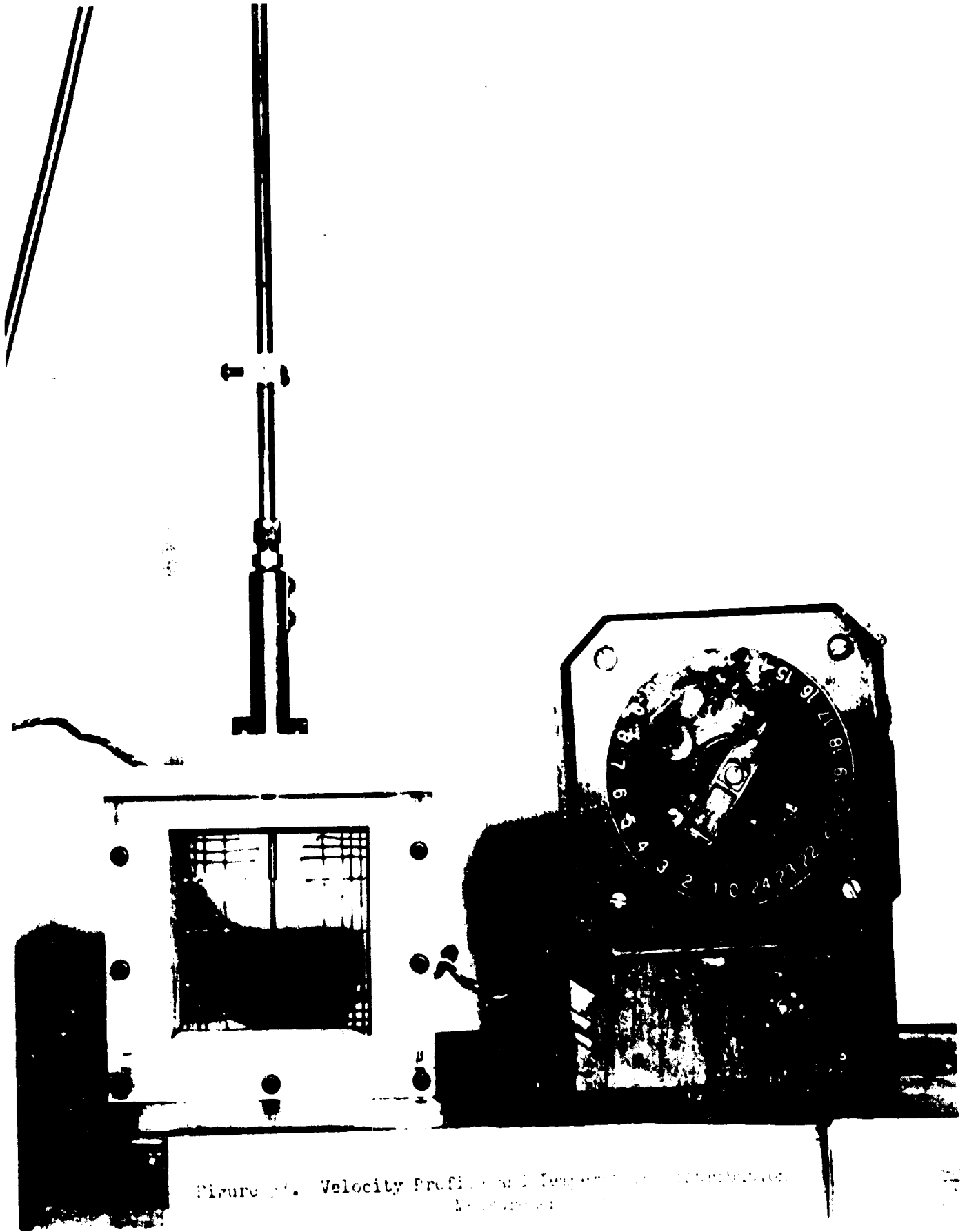


Figure 14. Velocity Profile and Temperature Distribution
Measurement

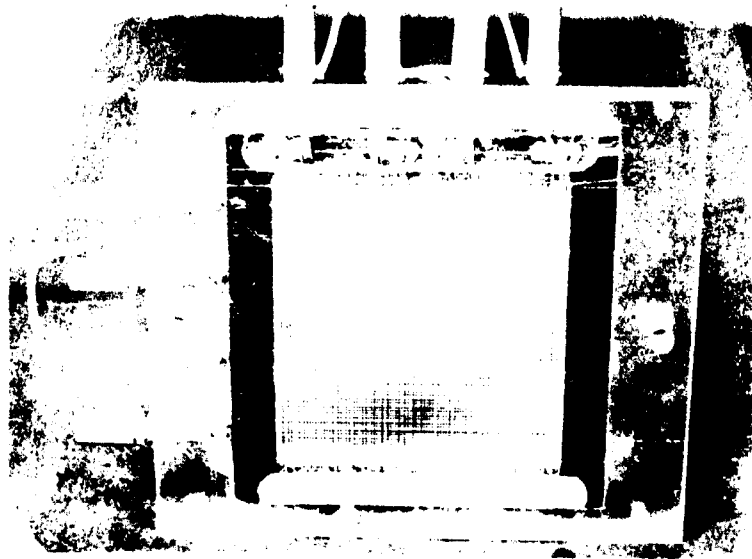
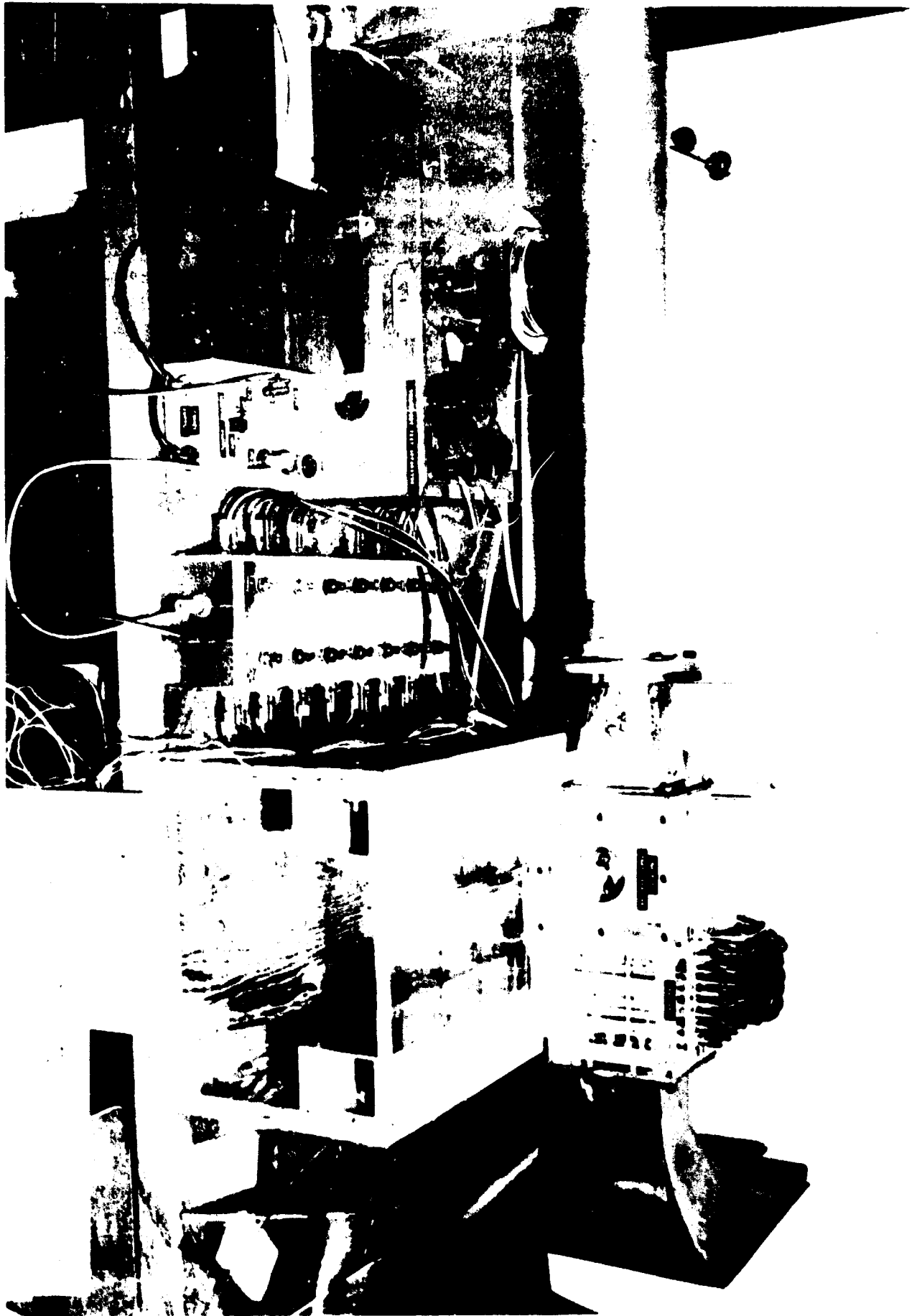


Figure 1. A photograph of a rectangular object, possibly a piece of equipment or a container, with a grid-like pattern on its front panel.



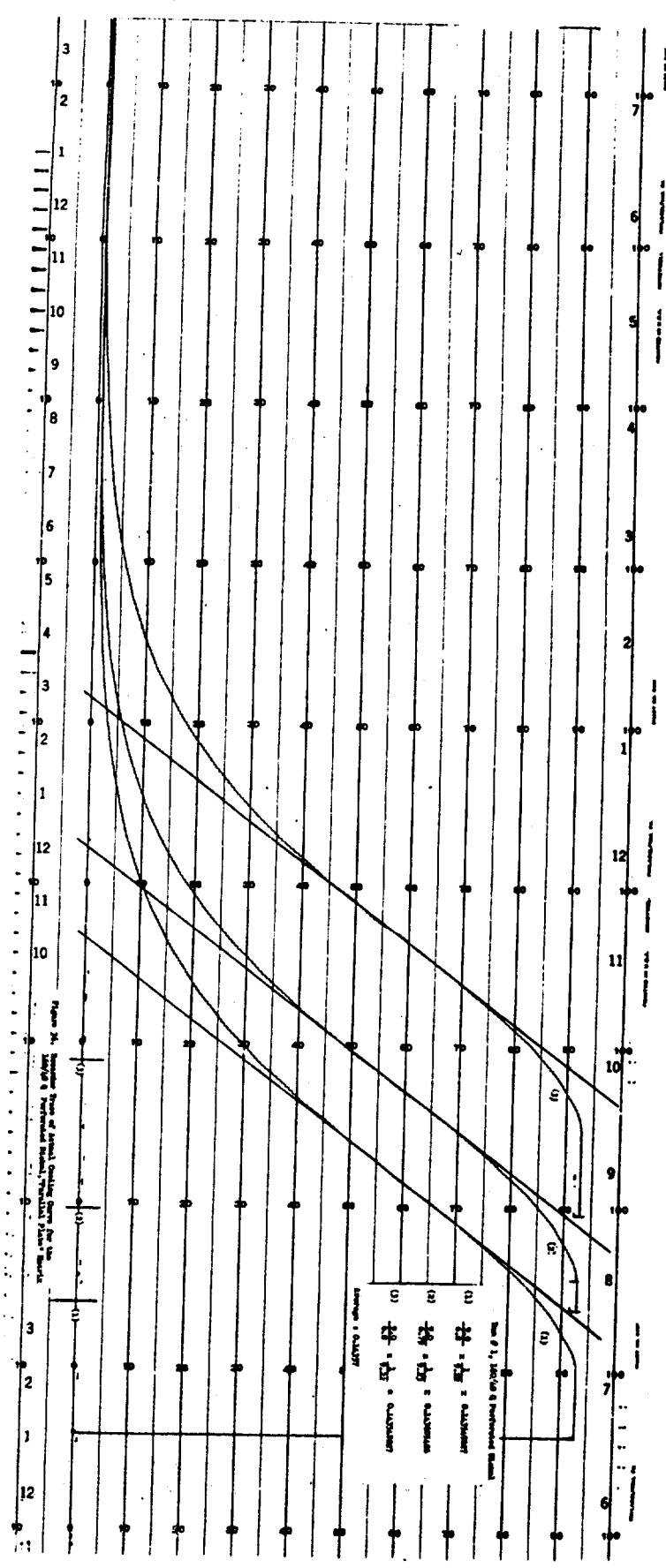


TABLE I SUMMARY OF HEAT TRANSFER AND FRICTION RESULTS:
160/40 TV PERFORATED NICKEL, MODIFIED PARALLEL PLATE

HEAT TRANSFER RESULTS				ISOTHERMAL FRICTION RESULTS					
RUN NO.	REYNOLD'S NUMBER N_R	$N_{St} N_{Pr}^{2/3}$	j	CONDUCTION PARAMETER λk	MAXIMUM SLOPE	N_{Tu}	$j' = j \times s$	REYNOLD'S NUMBER N_R	FRICTION FACTOR f
1	825.76	.00510	.00134	.54186	2.04	.00470	837.82	.02381	
2	655.96	.00788	.00169	.58496	3.15	.00726	665.67	.02971	
3	526.80	.01075	.00210	.64907	4.30	.00991	534.61	.03631	
4	404.33	.01260	.00273	.69503	5.04	.01161	410.22	.04337	
5	308.17	.01633	.00359	.77129	6.53	.01505	312.66	.05900	
6	204.31	.02375	.00543	.89956	9.50	.02189	207.29	.08664	
7	122.62	.03625	.00902	1.07060	14.50	.03341	124.41	.13255	
8	68.98	.0675*	.01604	1.1833	27.0*	.06218*	69.99	.23685	
9	38.79	.120*	.02851	1.1712	48.0*	.1105*	39.35	.42260	

* From Extrapolated Values of j versus N_R Curve

TABLE II SUMMARY OF HEAT TRANSFER AND FRICTION RESULTS:
160/40 Q PERFORATED NICKEL, MODIFIED PARALLEL PLATE

HEAT TRANSFER RESULTS				ISOTHERMAL FRICTION RESULTS				
RUN NO.	REYNOLD'S NUMBER N_{R}	$N_{St} N_{Pr}^{2/3}$	CONDUCTION PARAMETER λx	MAXIMUM SLOPE N_{Tu}	$j' = j x s$	REYNOLD'S NUMBER N_{R}	FRICTION FACTOR f	
1	911.23	.01217	.00094	.63507	4.05	.00980	924.54	.03686
2	744.10	.01427	.00116	.67558	4.75	.01150	754.96	.04080
3	597.40	.01478	.00144	.68555	4.92	.01191	606.12	.04931
4	458.68	.01953	.00188	.76765	6.50	.01574	465.38	.05785
5	351.29	.02389	.00245	.83415	7.95	.01925	356.42	.06954
6	230.65	.03531	.00373	.99130	11.75	.02845	234.01	.10424
7	138.84	.05077	.00618	1.15746	16.90	.04091	140.86	.15614
8	75.37	.07513	.01084	1.32066	25.00	.06054	80.53	.27078
9	43.37	.1370*	.01981	1.27471	45.6*	.1104*	44.01	.49671
10	18.41	.275*	.04667	1.05193	91.51*	.2216*	18.67	1.07260

* From Extrapolated Values of j versus N_{R} Curve

TABLE III SUMMARY OF HEAT TRANSFER AND FRICTION RESULTS:
125 μ PERFORATED NICKEL, MODIFIED PARALLEL PLATE

HEAT TRANSFER RESULTS				ISOTHERMAL FRICTION RESULTS					
RUN NO.	REYNOLD'S NUMBER N_R	$N_{St} N_{Pr}^{2/3}$	j	CONDUCTION PARAMETER λ_K	MAXIMUM SLOPE	N_{Tu}	$j' = j \times s$	REYNOLD'S NUMBER N_R	FRICTION FACTOR f
1	914.40	.00987	.00351	.59243	3.28	.00795	927.78	.03720	
2	747.25	.01044	.00429	.60382	3.47	.00841	758.19	.04033	
3	595.23	.01264	.00539	.64508	4.20	.01018	603.95	.04549	
4	460.47	.01496	.00697	.68852	4.97	.01205	467.21	.05310	
5	352.70	.01878	.00910	.75470	6.24	.01512	357.87	.06680	
6	229.81	.02661	.01395	.87198	8.84	.02143	233.17	.10051	
7	140.94	.03732	.02279	.97943	12.40	.03006	143.00	.14527	
8	80.37	.05222	.03996	1.04961	17.35	.04205	81.55	.23256	
9	43.68	.091*	.07341	1.01867	30.23*	.0733*	44.32	.41901	
10	18.87	.175*	.17002	.87812	58.14*	.1409*	19.15	.94158	

* From Extrapolated Values of j versus N_R Curve

TABLE IV SUMMARY OF HEAT TRANSFER AND FRICTION RESULTS:
125 P PERFORATED NICKEL, MODIFIED PARALLEL PLATE

HEAT TRANSFER RESULTS			ISOTHERMAL FRICTION RESULTS					
RUN NO.	REYNOLD'S NUMBER N_R	$N_{St} N_{Pr}^{2/3} j$	CONDUCTION PARAMETER λk	MAXIMUM SLOPE	N_{Tu}	$j' = j \times s$	REYNOLD'S NUMBER N_R	FRICTION FACTOR f
1	842.66	.00660	.00514	.55199	2.47	.00579	854.98	.02993
2	681.03	.00833	.00634	.58445	3.12	.00730	690.95	.03538
3	539.11	.01009	.00798	.62151	3.78	.00885	546.94	.04075
4	419.77	.01135	.01026	.65278	4.25	.00995	425.88	.04503
5	320.14	.01399	.01345	.70628	5.24	.01227	324.79	.05326
6	209.10	.02419	.02059	.87353	9.06	.02121	212.14	.07662
7	127.02	.03124	.03390	.94586	11.70	.02739	128.87	.11763
8	73.68	.0500*	.05873	.90270	18.73*	.04385*	74.76	.18271
9	40.24	.0990*	.10737	.83740	37.08*	.08681*	40.83	.32765
10	17.33	.2200*	.24936	.70783	82.40*	.19292*	17.58	.64335

* From Extrapolated Values of j versus N_R Curve

TABLE V SUMMARY OF HEAT TRANSFER AND FRICTION RESULTS:
50 G PERFORATED NICKEL, MODIFIED PARALLEL PLATE

HEAT TRANSFER RESULTS			ISOTHERMAL FRICTION RESULTS					
FROM REYNOLD'S NO.	REYNOLD'S NO. N_R	$N_{St} N_{Pr}^{2/3}$	CONDUCTION PARAMETER λ_K	MAXIMUM SLOPE	N_{Tu}	$j' = j \times s$	REYNOLD'S NUMBER N_R	FRICTION FACTOR f
1	1327.11	.01286	.00196	.57371	2.95	.00714	1346.50	.04157
2	1077.78	.01613	.00241	.61596	3.70	.00895	1093.53	.04656
3	860.44	.02049	.00302	.67115	4.70	.01137	873.01	.05366
4	660.25	.02167	.00393	.68872	4.97	.01203	669.90	.05654
5	505.10	.02315	.00511	.70620	5.31	.01285	512.43	.06639
6	332.27	.03575	.00777	.84294	8.20	.01984	337.09	.09211
7	202.59	.05275	.01274	.98835	12.10	.02927	205.54	.12593
8	116.91	.06932	.02207	1.06986	15.9	.03847	118.61	.21087
9	63.60	.1250*	.04050	1.04240	28.7*	.0694*	64.52	.37091
10	27.24	.2740*	.09455	.90406	62.8*	.1521*	27.63	.80961

* From Extrapolated Values of j -versus N_R Curve

TABLE VI SUMMARY OF HEAT TRANSFER AND FRICTION RESULTS:
160/40TV PERFORATED NICKEL FIN, SOLID SPLITTERS "PARALLEL PLATE"

HEAT TRANSFER RESULTS:			ISOTHERMAL FRICTION RESULTS:			
RUN NO.	REYNOLD'S NUMBER N_R	$M_{st} N_p f$ j	CONDUCTION PARAMETER λ_k	MAXIMUM SLOPE N_{tu}	REYNOLD'S NUMBER N_R	FRICTION FACTOR f
1	765.94	.00695	.00451	.56963	777.13	.02908
2	629.02	.00874	.00549	.61108	638.20	.03313
3	495.98	.01125	.00696	.67109	503.22	.04111
4	385.97	.01307	.00895	.71202	391.60	.04730
5	291.98	.01561	.01179	.76775	296.23	.06052
6	192.67	.02311	.01787	.88931	195.47	.08737
7	118.00	.03412	.02920	1.00846	119.47	.12713
8	67.44	.055*	.05110	.93807	68.42	.20821
9	36.73	.0923*	.09375	.85417	37.26	.35804
10	15.91	.190*	.21648	.76567	16.14	.78018

* From Extrapolated Values of j versus N_R Curves

TABLE VII SUMMARY OF HEAT TRANSFER AND FRICTION RESULTS:
SOLID NICKEL, "PARALLEL PLATE"

ISOTHERMAL FRICTION RESULTS:

HEAT TRANSFER RESULTS:

2/3

RUN NO.	REYNOLD'S NUMBER N_R	$N_{St} N_{Pr}$	j	CONDUCTION PARAMETER λ	MAXIMUM SLOPE	N_{Tu}	REYNOLD'S NUMBER N_R	FRICTION FACTOR f
1	729.78	.00667	.00995	.57372	2.85	740.42	.02836	
2	600.20	.00737	.01209	.58983	3.15	608.95	.03389	
3	474.84	.00842	.01527	.61607	3.60	481.75	.04027	
4	368.55	.01093	.01969	.67998	4.67	373.92	.04731	
5	282.69	.01278	.02567	.72287	5.46	286.81	.05896	
6	184.45	.01825	.03934	.82225	7.80	187.14	.08669	
7	113.77	.02258	.06376	.86518	9.65	115.43	.12779	
8	64.14	.0375*	.11308	.81509	16.02*	65.08	.21281	
9	35.21	.059*	.20603	.77453	25.2*	35.72	.37241	

* From Extrapolated Values of j versus N_R Curve

TABLE VIII SUMMARY OF HEAT TRANSFER AND FRICTION RESULTS:
1.60/40TV PERFORATED NICKEL, 20° SKEN

HEAT TRANSFER RESULTS:			ISOTHERMAL FRICTION RESULTS:					
RUN NO.	REYNOLD'S NUMBER N_{R}	$N_{St} N_{Pr}^{2/3}$	CONDUCTION PARAMETER λ_K	MAXIMUM SLOPE	N_{Tu}	$j' = j \times s$	REYNOLD'S NUMBER N_R	FRICTION FACTOR f
1	961.20	.00563	.00114	.53466	1.70	.00189	975.26	.03544
2	330.66	.00976	.00132	.57513	2.95	.00327	842.79	.04105
3	735.32	.01165	.00149	.60684	3.52	.00390	746.00	.04399
4	625.93	.01400	.00176	.64507	4.23	.00469	635.11	.05018
5	456.99	.01953	.00241	.73691	5.90	.00654	463.70	.07026
6	365.31	.02105	.00300	.76108	6.36	.00705	370.64	.07379
7	241.54	.03178	.00453	.90357	9.60	.01065	245.05	.10837
8	146.02	.04800	.00750	1.07054	14.5	.01608	148.15	.16407
9	83.40	.09100*	.01313	1.22320	27.5*	.03049*	84.61	.26504
10	47.02	.1570*	.02328	1.28233	47.4*	.05261*	47.70	.46809
11	23.80	.3100*	.04599	1.12518	93.6*	.1029*	24.15	.92250

*From Extrapolated Values of j versus N_R Curve

APPENDIX A

DATA REDUCTION RELATIONSHIPS

Summarized herein are those data reduction relationships which are of prime importance in obtaining the heat transfer and flow friction characteristics as presented from the raw data taken. Before the data on the matrices tested can be reduced, or a comparison of the different matrices can be made, it is essential to obtain accurate geometrical dimensions. The geometrical factors of interest are the porosity, p , the hydraulic diameter, D_H , and the area compactness, β . Determination of any of these fixes the third since it may be shown [11] that

$$\beta = \frac{4p}{D_H} \quad (A-1)$$

The definitions of these terms are:

$$(1) \quad p = \frac{\text{Free Flow Area}}{\text{Frontal Area}} = \frac{A_c}{A_{fr}} \quad (A-2)$$

$$(2) \quad D_H = \frac{4 \times \text{Free Flow Area}}{\text{Heat Transfer Surface Area}} = 4 \frac{A_c}{A} L \quad (A-3)$$

$$(3) \quad \beta = \frac{\text{Heat Transfer Surface Area}}{\text{Frontal Area} \times \text{Flow Length}} = \frac{A}{A_{fr} L} \quad (A-4)$$

MAXIMUM SLOPE

The maximum slope of the generalized cooling curve is a unique function of N_{Tu} and λ [10].

$$\frac{d \left[\frac{t_{f2} - t_1}{t_{f1} - t_1} \right]}{d \left[\tau / N_{Tu} \right]_{\max}} = \phi(N_{Tu}, \lambda) \quad (A-5)$$

τ and N_{Tu} have both been previously defined, but for convenience the relationships are restated:

$$\tau \approx \frac{hA}{W_s c_s} \theta \quad \text{and} \quad N_{Tu} = \frac{hA}{\dot{m} c_p}$$

Therefore:

$$\tau/N_{Tu} = (\dot{m} c_p / W_s c_s) \theta$$

and

$$d(\tau/N_{Tu}) = (\dot{m} c_p / W_s c_s) d\theta = (C/\bar{C}_s) d\theta \quad (A-6)$$

Furthermore:

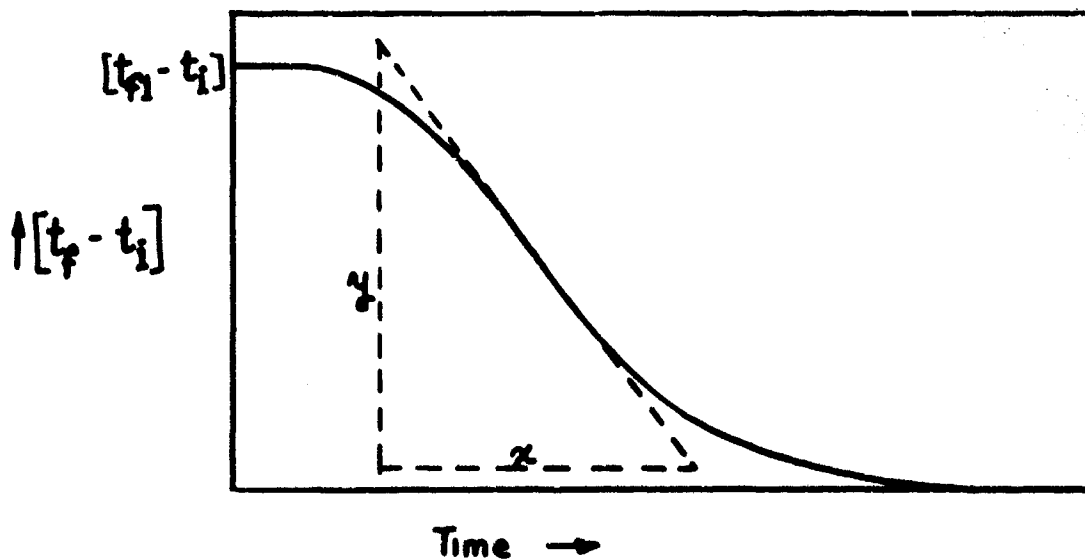
$$\frac{t_{f2} - t_i}{t_{f1} - t_i} = \frac{t_{f2} - t_{f1}}{t_{f1} - t_i} + 1 \quad [7]$$

and

$$d \left[\frac{t_{f2} - t_i}{t_{f1} - t_i} \right] = \frac{1}{t_{f1} - t_i} d [t_{f2} - t_{f1}] \quad (A-7)$$

Combining (A-6) and (A-7)

$$d \left[\frac{t_{f2} - t_i}{t_{f1} - t_i} \right]_{\max} = \frac{\bar{C}_s}{C} \frac{1}{t_{f1} - t_i} \frac{d[t_{f2} - t_{f1}]}{d\theta} \quad (A-8)$$



From the above sketch

$$(1) \frac{d[t_{f2}-t_{f1}]}{d\theta} \Big|_{\max} = \frac{y}{x}$$

$$(2) \frac{x}{\text{Chart speed}} = d\theta, \text{ sec}$$

$$(3) y = d(t_{f2}-t_{f1}), \text{ inches}$$

$$(4) M = (t_{f1}-t_i), \text{ inches}$$

Combining these determined values into (A-8) yields:

$$\frac{d \left[\frac{t_{f2}-t_i}{t_{f1}-t_i} \right]}{d[\tau/N_{tu}]} \Big|_{\max} = \frac{\bar{C}}{C} \cdot \frac{1}{M} \cdot \frac{y}{x} \cdot \text{Chart speed} \quad (\text{A-9})$$

With this value of maximum slope and $\lambda = \frac{k A}{mc L} \frac{s}{p}$, enter TABLE I or Figure 4 of Howard [5] or Figure 2-A of Howard [4] to obtain a corresponding N_{tu} value.

MASS RATE OF FLOW:

The mass rate of flow is calculated from the method given in reference [14] with necessary rearrangements in order to reduce unnecessary hand calculations and to gain the full benefits of Murdock [13]:

$$\dot{m} = 359Kd_o^2 F_a Y \sqrt{\Delta P_o \gamma} \quad (\text{A-10})$$

where: K = flow coefficient, including velocity of

approach = $\frac{C}{\sqrt{1-\beta_o^4}}$ with C = orifice coefficient of discharge (obtained from [13]) and

β_o = ratio of orifice diameter to internal pipe (β in [4]) diameter, d_o/d

d_o = orifice diameter, inches

F_a = thermal expansion factor

Y = expansion factor

γ = specific weight of fluid flowing = $\frac{P}{RT}$ with P in lbf/ft².

$$R = 53.35 \text{ (ft-lbf)/(lbm-}^\circ\text{R)}$$

$$T = t(^{\circ}\text{F}) + 459.7 = \text{degrees Rankine (}^\circ\text{R)}$$

ΔP_o = Pressure drop across the orifice, inches H_2O substituting $\frac{P}{RT}$ for γ , since the magnitude of the local acceleration of gravity, g , is taken as being equal to the magnitude of standard acceleration of gravity, g_c ; and $\frac{C}{\sqrt{1-\beta_o^4}}$ for K gives:

$$\dot{m} = \frac{359C}{\sqrt{1-\beta_o^4}} d_o^2 F_a Y \sqrt{\Delta P_o} \cdot \frac{P}{RT} \quad (\text{A-11})$$

Inserting the numerical value for R and converting P to units of lb/in^2 yields:

$$\dot{m} = \frac{589.81 \text{ Cd}_o^2 F_a Y}{\sqrt{1-\beta_o^4}} \sqrt{\Delta P_o} \cdot \frac{P(\text{psia})}{RT} \quad (\text{A-12})$$

From Figure 38, reference [14]: $F_a \approx 1.00$

From Figure 40b, reference [14]: $Y = 0.9985 \approx 1.0$

The pressure, P , in (A-12), is hereafter referred to as P_3 and is determined by the following relationship:

$$P_3 = (P_{\text{atm}} - P_o/13.6) 0.4912, \text{ lb}/\text{in}^2 \quad (\text{A-13})$$

Where P_{atm} is the atmospheric pressure in inches of mercury,

P_o is the static pressure upstream of the orifice in inches of H_2O

13.6 inches of H_2O /inch of mercury

0.4912 (lb/in^2)/inch of mercury

The temperature, T , in (A-12) is the air temperature at the orifice in degrees Rankine (T_o):

$$T_o = t_o + 459.7 \quad (\text{A-14})$$

Replacing F_a and Y in (A-12) with their numerical values, the equation reduces to the working form:

$$\dot{m} = \frac{589.81 C d_o^2}{\sqrt{1-\beta^4}} \sqrt{\Delta P_o \cdot \frac{P_3}{T_o}} \quad \text{lbm/hr} \quad (\text{A-15})$$

REYNOLDS NUMBER:

Reynolds number is defined as:

$$N_R = \frac{D_H G}{\mu} \quad (\text{A-16})$$

where G is the mass flow velocity based on the free flow area, A_c .

$$G = \frac{\dot{m}}{A_c} = \frac{\dot{m}}{p A_{fr}} \quad (\text{A-17})$$

Substituting (A-17) into (A-16):

$$N_R = \frac{\dot{m}}{\mu A_{fr}} \frac{D_H}{p} \quad (\text{A-18})$$

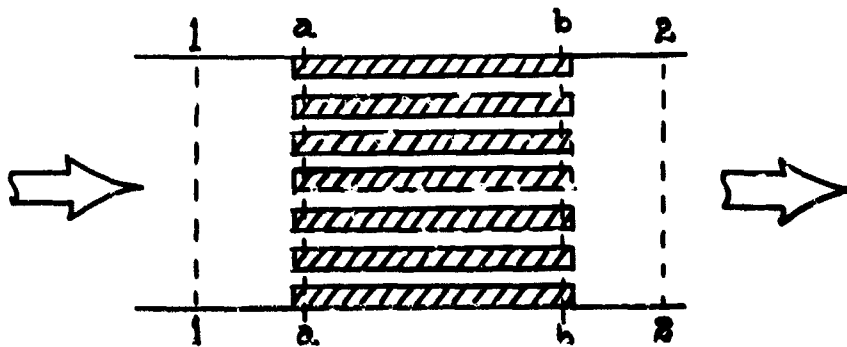
But from (A-1) $D_H/p = \frac{4}{\beta}$, therefore: $N_R = \frac{4\dot{m}}{\mu A_{fr}} \frac{1}{\beta}$ (A-19)

Equation (A-19) shows that for a given matrix and mass flow rate the Reynolds number is inversely proportional to the compactness. Substituting (A-4) into (A-19) yields the working equation:

$$N_R = \frac{4L\dot{m}}{\mu A} \quad (\text{A-20})$$

FANNING FRICTION FACTOR

The following sketch together with equation (A-21) describes the flow system under consideration: [8]



$$\frac{\Delta P}{P_1} = \frac{G^2}{2g_c} \frac{v_1}{P_1} \left[\underbrace{(K_c + 1 - p^2)}_{\text{entrance effect}} - 2 \underbrace{\left(\frac{v_2}{v_1} - 1 \right)}_{\text{flow acceleration}} + f \underbrace{\frac{A}{A_c} \frac{v_1}{v_1}}_{\text{core friction}} - \underbrace{(1 - p^2 - K_e)}_{\text{exit effect}} \frac{v_2}{v_1} \right] \quad (\text{A-21})$$

It is important to note that $v_a \approx v_1$ and $v_b \approx v_2$ in the above sketch as the pressure changes (for gas flow heat exchanger application) from section 1 to a and b to 2, respectively, are very small relative to the total pressure. Inasmuch as the testing is performed with air at moderate temperatures and pressures, the perfect gas law is applicable ($P = \rho RT$).

Substituting $v = \frac{1}{\rho}$ and recalling that $\frac{D_H}{4L} = \frac{A_c}{A}$ or $\frac{r_H}{L} = \frac{A_c}{A}$ from equation (A-3), equation (A-21) solved for f for the isothermal case becomes:

$$f = \left[2g_c \rho_m \frac{\Delta P}{G^2} - \frac{P_1 + P_2}{2} \left(\frac{K_c}{P_1} + \frac{K_e}{P_2} \right) - \frac{P_1 + P_2}{2} \left(\frac{1}{P_2} - \frac{1}{P_1} \right) (1+p^2) \right] \frac{r_H}{L} \quad (A-22)$$

where $\rho_m = \frac{\rho_1 + \rho_2}{2}$ with the upstream values subscripted by 1 and the downstream subscripted by 2. K_c is the entrance coefficient and K_e the exit coefficient, and both are dependent on porosity, shape of the flow cross section, and the matrix Reynolds number. Values of K_c and K_e are obtained from Figures 5-3, -4, -5 of reference [8].

If we consider an order of magnitude approximation, the first term in (A-22) is by far the greatest contributor to friction factor for small pressure differentials.

The approximation, therefore, that $\frac{P_1 + P_2}{2} = P_m \approx P_1 \approx P_2$ reduces (A-22) to the following

$$f = \left[2g_c \rho_m \frac{\Delta P}{G^2} - (K_c + K_e) + \frac{\Delta P}{P_m} (1+p^2) \right] \frac{r_H}{L} \quad (A-23)$$

London [11] points out that the relationships given here can be recombined in such a manner so as to show that f is proportional to the porosity cubed and inversely proportional to the compactness ($f \propto p^3/\beta$).

COLBURN j FACTOR:

Colburn j factor is defined as:

$$j = N_{St} N_{Pr}^{2/3} = \frac{h}{G c_p} N_{Pr}^{2/3} \quad (A-24)$$

Substituting (A-17) for G and multiplying by A/A yields

$$j = \frac{hA}{mc_p} \frac{A_c}{A} N_{Pr}^{2/3} \quad (A-25)$$

but $\frac{hA}{mc_p} = N_{Tu}$

therefore:

$$j = N_{Tu} \frac{A_c}{A} N_{Pr}^{2/3} \quad (A-26)$$

Combining equations (A-1) and (A-3):

$$\frac{A_c}{A} = \frac{\phi}{\beta L}$$

thus:

$$j = N_{Tu} N_{Pr}^{2/3} \frac{1}{L} \frac{\phi}{\beta} \quad (A-27)$$

It is apparent from equation (A-27) that the Colburn j factor is directly proportional to porosity and inversely proportional to compactness ($j\phi/\beta$).

HEAT TRANSFER POWER AND FLOW FRICTION POWER:

An evaluation of the heat transfer power versus flow friction power is of interest in that it is a measure of relative performance.

The heat transfer power per unit area per degree temperature difference is [8]:

$$h = \frac{c_p \mu}{N_{Pr}^{2/3}} \frac{1}{D_H} j N_R \quad (A-28)$$

Equation (A-28) with the properties evaluated at standard conditions of dry air at 500°F and one atmosphere becomes:

$$h_{STD} = 0.02195 \left(\frac{1}{D_H} \right) (N_{Rj}) \text{ Btu/hr ft}^2 \text{ } ^\circ\text{F} \quad (\text{A-29})$$

where

$$c_p = 0.2477 \text{ Btu/lbm } ^\circ\text{F}$$

$$\mu = 0.0678 \text{ lbm/hr ft}$$

$$\rho = 0.0413 \text{ lbm/ft}^3$$

$$N_{Pr} = 0.671$$

The flow friction power per unit area is [8]:

$$E = \frac{1}{2g_c} \frac{\mu^3}{\rho^2} \left(\frac{1}{D_H} \right)^3 f N_R^3 \quad (\text{A-30})$$

When equation (A-30) is evaluated at standard conditions (μ and ρ values given above), the flow friction power per unit area at standard conditions is:

$$E_{STD} = 1.11 \times 10^{-7} \left(\frac{1}{D_H} \right)^3 f \left(\frac{N_R}{1000} \right)^3 \text{ HP/ft}^2$$

For comparison purposes the surface geometries were reduced to a common hydraulic diameter of $D_H = 2 \times 10^{-3}$ ft.

APPENDIX B

DESCRIPTION OF EQUIPMENT

Heat transfer data was obtained utilizing the "single blow" technique which consists briefly of monitoring the fluid temperature response at the test matrix exit while subjecting the inlet to the test matrix to a step change in fluid temperature.

Friction factor was determined from pressure drop data obtained from static pressure taps located in the test section - one at inlet, the other at the exit.

Necessary equipment to perform such an experiment falls into one of the following categories:

- (1) Fluid source
- (2) Flow metering system
- (3) Temperature measuring system
- (4) Pressure measuring system
- (5) Fluid heater system
- (6) Matrix holder and test section casing

FLUID SOURCE:

Air, the working fluid, was provided to the test apparatus by connecting the rig to the inlet of a 30HP, multistage, Spencer Turbo-Compressor rated for 550cfm operating on a 220 volt a.c. power supply.

FLOW METERING SYSTEM: (See Figure 1)

The flow metering system consisted of an ASME standard orifice section constructed for d and $d/2$ pressure taps in a 3.08" inside diameter metal tube. [14]. A wide flow range was obtained by utilizing thin

plate concentric orifices of throat diameter 2.310, 1.971, 1.232, 1.540, 0.462, and 0.308 inches respectively.

Control of the pressure drop across the orifice was maintained by a gate valve downstream of the apparatus, ahead of the compressor inlet and another gate valve on the compressor inlet. The blast gate on the compressor discharge was pre-set so that the unit could not be operated beyond the full load rating of the turbo.

TEMPERATURE MEASURING SYSTEM: (See Figure 1)

The majority of the temperatures were measured with iron-constantan thermocouples. These thermocouples use iron for the positive conductor and constantan for the negative conductor. Measuring T_1 is a group of five thermocouples in series, bound together and insulated from each other by teflon tape and inserted in a 1/8" diameter aluminum tube to serve as a radiation shield. A small aperture was cut in the inserted tube facing upstream. T_2 and T_4 are five wire thermocouple grids, connected in series, mounted permanently in the test section casing. T_3 is a movable five wire series connected thermocouple grid located in the matrix holder so that it is adjacent to the downstream side of the matrix. The purpose of connecting the thermocouples in series was to magnify the emf output so that the instrument sensitivity to small temperature changes would be enhanced. With T_2 bucked against T_4 , it is possible to determine the temperature uniformity across the matrix. T_1 versus T_3 indicates the difference between upstream and downstream temperatures; thus, it is this combination which is used to record the rate of change of upstream and downstream temperatures with time, resulting from the step change in fluid temperature upstream. This differential

is recorded on a Minneapolis-Honeywell "Brown" Recorder and serves as the primary data for heat transfer evaluation of the matrix. The recorder has variable chart speeds so that acceptable cooling curves for maximum slope determination can be generated. This instrument has a span adjustment which permits the span to be varied continuously from the narrowest to the widest span desired from 0 to 55 millivolts. For the work performed herein, the recorder was precalibrated for a 0 - 3 millivolt scale. This unit also has adjustable suppression and damping adjustment features. The damping adjustment provides a filter network for removing a.c. strays, and provides correct damping so that neither undershoot nor overshoot in the response curves is experienced.

A copper constantan thermocouple was inserted into the duct just ahead of the orifice to measure T_o , orifice temperature. This temperature was read in millivolts on a Rubicon Company Portable Precision Potentiometer, converted to degrees Fahrenheit and recorded for each run.

A copper constantan thermocouple grid was inserted in place of T_3 to determine the temperature distribution across the cross section during initial check out of the apparatus. This thermocouple arrangement was part of a special holder lined with balsa wood to provide a smooth, continuous flow passage, which also contained an impact tube used for checking the velocity profiles (See Figure 33).

PRESSURE MEASURING SYSTEM: (See Figure 1)

Pressure taps are located upstream and downstream of the matrix and on either side of the orifice. Each tap is connected to an appropriate manometer or draft gage via Imperial Company "poly-flo" tubing. Quick closing valves were installed at various positions in the line to permit isolation of sections and as a safety feature.

The following instruments were utilized:

- (1) Meriam Instrument Company, 0 - 50" manometer
- (2) Meriam Instrument Company, -8" to +8" manometer
- (3) Ellison Differential Direct Draft Gages, 0 - 6", 0 - 8"
- (4) Ellison Inclined Draft Gages, 0 - 0.5", 0 - 6".
- (5) E. Vernon Hill and Company Type "C" Micromanometer,
0 - 1.25".

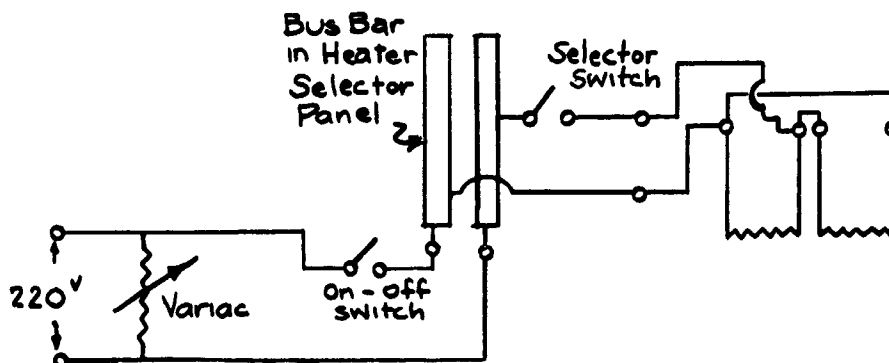
Any one of these instruments or a combination can be used to measure the differential pressures of the orifice or matrix or the required static pressures - upstream of matrix and upstream of the orifice. Cross checking of the various instruments assured reliable operation.

FLUID HEATER SYSTEM: (See Figure 1)

The heater section is comprised of 28 nichrome wire heaters of 0.0031" diameter. The heater system was designed to elevate the air temperature 20°F above ambient for a mass rate of flow of 1000 lb/hour. The nichrome material was selected because it has high resistivity, low thermal conductivity and specific heat, and has a very small time constant so that it permits one to approach the idealized step function.

The wire heaters are wound two to a bakelite frame, 1/32" between each wire, with 50 and 52 wires respectively to each heater on a frame. These heaters are connected in parallel, then via a switch to a variable voltage bus. The heater frame and its electrical connections are apparent in Figures 34 and 35.

A schematic wiring diagram for one of the two heater complexes is shown below. A total of 14 frames are wired in this fashion, thereby putting all 28 heaters in parallel, permitting two to be switched on or off at a time.



The number of heaters in use decreases as flow rate decreases. The necessary voltage variations are obtainable by a General Radio Company Type W20HM "Variac" Autotransformer, 0 - 280 volt, 8 amp load from a 240 volt 50 - 60 cycle line.

MATRIX HOLDER AND TEST SECTION: (See Figures 31, 32, and 35)

The matrix holder and test section are made of polyethylene plastic. The test section casing holds the T_2 and T_4 thermocouple grids permanently mounted, as well as the upstream and downstream static pressure taps required for determining friction factor. All parts were machined to close tolerance to assure a snug fit for the matrix holder and to guarantee good alignment of the flow channel through the heater and test sections. The flow channel is $3 - 3/16'' \times 3 - 3/16''$ and matrices of flow lengths up to 3" may be tested. As mentioned previously under Temperature Measuring System, the T_3 thermocouple grid is located in the matrix holder.

Correct positioning of the test matrices in the flow channel is ensured by using styrofoam plastic inserts. The inlet cone and stainless steel 60 mesh screen employed provided a uniform velocity to the heater section.

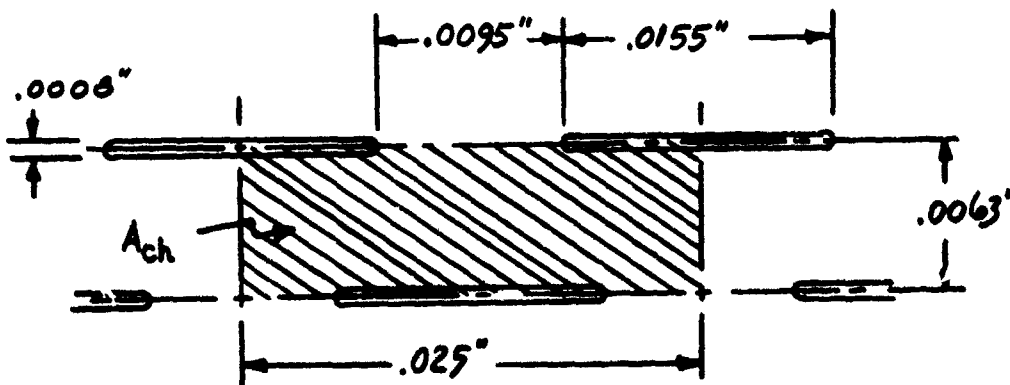
APPENDIX C

PERFORATED NICKEL GEOMETRIC PROPERTIES

The material used in the perforated plate matrices was pure nickel, electro-deposited sheet of integral structure manufactured by Perforated Products, Incorporated. Types 160/40TV, 160/40Q, 50G, 125M and 125P were utilized in the matrices - the first two of these having slotted openings and the remaining three having round openings. A brief description of each of the aforementioned types as specified by the manufacturer is set forth in Table C-1.

Inasmuch as the perforations in all cases were conical, the use of the average slot length or average hole diameter was considered a propos. Close examination of each of the different types revealed that this average value was somewhat less than the dimensions specified by the manufacturer in each case. In addition to the requirement for determining porosity of the plate, a correction for the increased longitudinal conduction length due to the perforations as well as a correction to the solid conduction cross-sectional area was performed. The following idealized patterns for each type used, best illustrate these corrections.

160/40TV



12

Cross Hatched Area, $A_{ch} = (.0063)(.025) = .0001575 \text{ in.}^2$

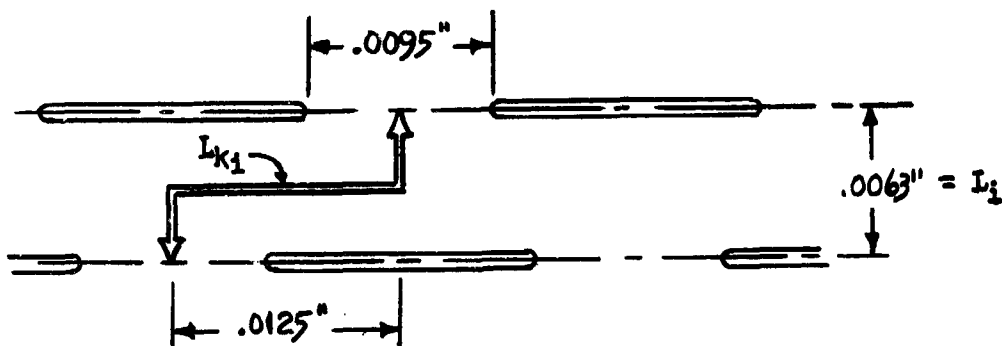
Slotted Area, A_{sl} , in $A_{ch} = (.0008)(.0155) = .0000124 \text{ in.}^2$

Plate Porosity, the fraction of open or slotted area,

$$v = \frac{A_{sl}}{A_{ch}}$$

Solidity, s , is $1 - v = 1 - \frac{A_{sl}}{A_{ch}}$

$$s = 1 - \frac{.0000124}{.0001575} = 0.9212$$



L_{k1} , conduction path length, $= 0.0125 + 0.0063 = 0.0188''$

$$\frac{L_i}{L_{k1}} = \frac{.0063}{.0188} = 0.3351$$

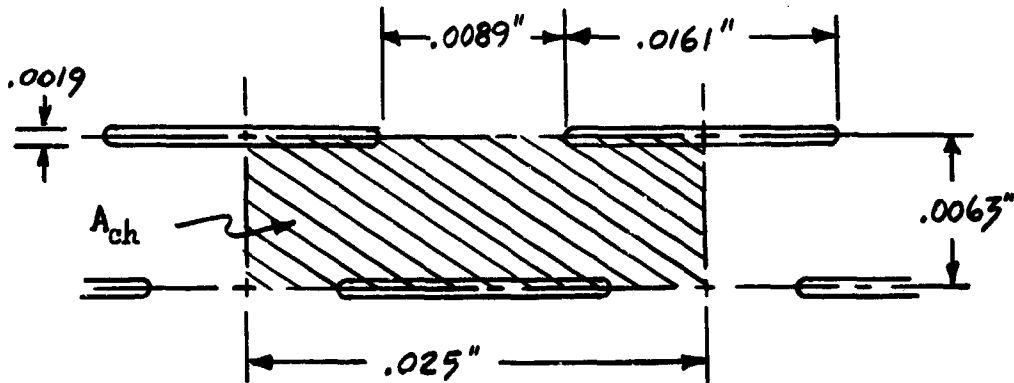
The solid cross sectional area for heat conduction, A_{k_i} varies along the path length. The area, A_{k_i} , selected was the cross sectional area between the slots normal to the flow direction, i.e.,

$$A_{k_i} = (0.0095)(0.0022) = 0.0000209 \text{ in.}^2$$

Just as $L = \Sigma L_i$ where L is the total matrix flow length and L_i is the flow length between two successive perforations; so does $L_k = \Sigma L_{k_i}$ and $A_k = \Sigma A_{k_i}$. In evaluating A_k , a conduction area reduction ratio is employed and is defined as $\zeta = \frac{\text{cross sectional area of perforations}}{\text{cross sectional area}}$; therefore, A_k is the solid cross sectional area multiplied by $1 - \zeta$ i.e.,

$$\begin{aligned}
 A_k &= A_s (1-\zeta) \\
 &= 1.6058 \left(1 - \frac{(.0155)(.0022)}{(.025)(.0022)} \right) = 0.6102 \text{ in}^2 \\
 &= 0.00424 \text{ ft}^2
 \end{aligned}$$

160/40Q



$$A_{ch} = (.0063)(.025) = .0001575 \text{ in}^2$$

$$A_{s1} = (.0019)(.0161) = .00003059 \text{ in}^2$$

$$\zeta = .655$$

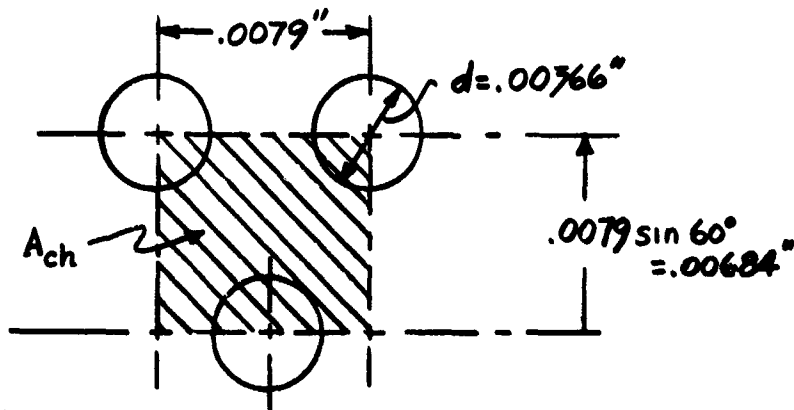
$$v = .1942$$

$$A_k = A_s (1-\zeta) = .002887 \text{ ft}^2$$

$$s = .8058$$

$$\frac{L}{L_k} = 0.3351, \text{ same as } 160/40TV$$

125M

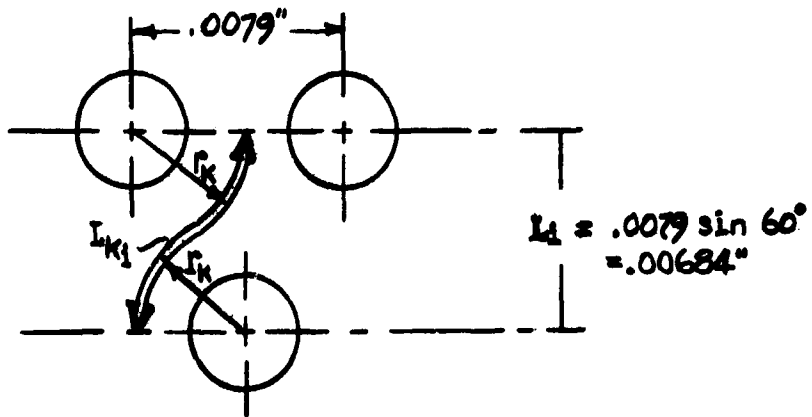


$$A_{ch} = (.00684)(.0079) = .00005404 \text{ in}^2$$

$$v = \frac{A_{hole}}{A_{ch}} = \frac{.00001052}{.00005404} = 0.19466$$

$$A_{hole} = \frac{\pi}{4} (.00366)^2 = .00001052 \text{ in}^2$$

$$s = .8053$$



The equivalent conduction length, L_{k_1} , is computed in the case of round perforations assuming the path to be as shown above, i.e., $\frac{2\pi r_k}{3}$ where r_k is the radial distance equal to one-half the center to center distance. Thus

$$L_{k_1} = \frac{2\pi (.0079)}{3} = .00827''$$

and

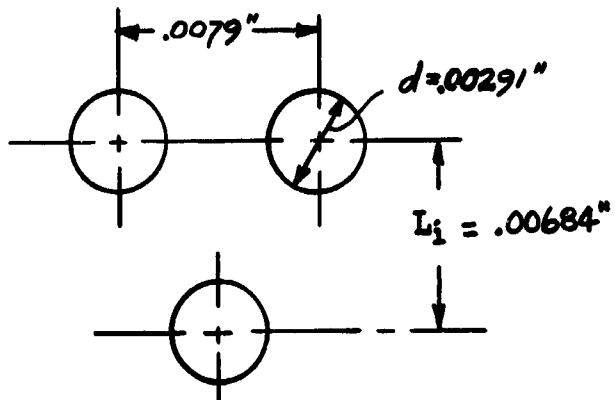
$$\frac{L_1}{L_{k_1}} = \frac{.00684}{.00827} = .82709$$

A_k is determined as in the case of the slotted perforations.

$$\begin{aligned} \zeta &= \frac{\text{diam. of hole} \times \text{plate thickness}}{\text{center to center distance} \times \text{plate thickness}} \\ &= \frac{(.00366)(.0016)}{(.0079)(.0016)} = .4633 \end{aligned}$$

$$\begin{aligned} \text{Therefore, } A_k &= A_g (1-\zeta) = 1.1679 \text{ in.}^2 (1-.4633) \\ &= .6268 \text{ in.}^2 = .00435 \text{ ft.}^2 \end{aligned}$$

125P



$$A_{ch} = (.00684)(.0079) = .00005404 \text{ in}^2$$

$$A_{hole} = \frac{\pi}{4} (.00291)^2 = .00000665$$

$$A_k = A_s(1-\zeta) = .00640 \text{ ft}^2$$

$$v = 0.12307$$

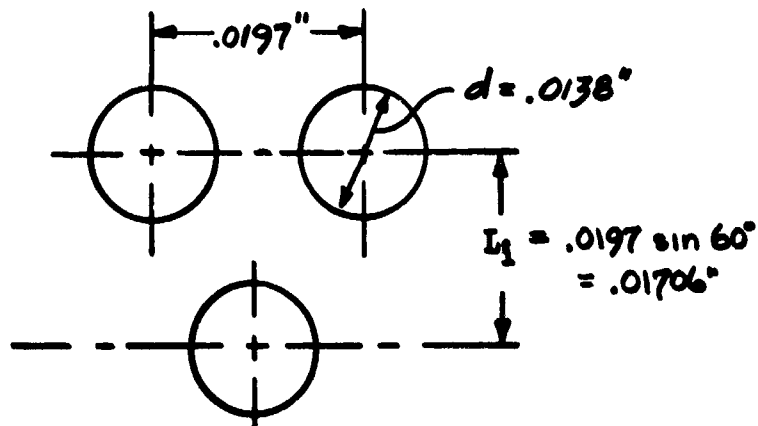
$$s = 0.8769$$

$$L_{ki} = .00827''$$

$$\frac{L_i}{L_{ki}} = .82709$$

$$\zeta = 0.3684$$

50G



$$A_{ch} = (.01706)(.0197) = .00033608 \text{ in}^2$$

$$A_{hole} = \frac{\pi}{4} (.0138)^2 = .00014957 \text{ in}^2$$

$$\frac{L_i}{L_{ki}} = .82697$$

$$v = .44504$$

$$s = .55496$$

$$L_{ki} = .02063''$$

$$\zeta = .7005$$

$$A_k = A_s(1-\zeta) = .00243 \text{ ft}^2$$

Type	Opening	Hole Diameter (inches)	Plate Thickness (inches)	Center to Center Distance, (inches)	% Open Area
160/40TV	slotted	0.0008 x 0.017	0.0022	0.0063 x 0.025	12.0
160/40Q	slotted	0.0019 x 0.018	0.0016	0.0063 x 0.025	24.5
50G	round	0.0145	0.0016	0.020	50.0
125M	round	0.0039	0.0016	0.0079	22.5
125P	round	0.003	0.002	0.0079	14.5

TABLE C-1 Geometric Properties of Perforated Nickel

APPENDIX D

SAMPLE CALCULATIONS

The following sample calculations are based on data obtained from Run #1 for the modified parallel plate matrix constructed from the 160/40Q perforated nickel material. The basic geometric parameters are illustrated in Appendix A.

Prior to the reduction of data, several fixed parameters must be evaluated.

DIMENSIONS OF FINNED SHEETS: 3.9375" x 2.00" x .0016"
(before forming)

DIMENSIONS OF SPLITTER PLATES: 3.1875" x 2.00" x .0016"

NUMBER OF FINNED SHEETS: 102

NUMBER OF SPLITTER PLATES: 103

WEIGHT OF MATRIX: 311.0979 gms/453.6 gm/lb = 0.68584 lb.

MATERIAL CONSTANTS:

$$k_s = 38.7 \text{ Btu/hr } ^\circ\text{F} - \text{ft}$$

$$c_s = 0.1065 \text{ Btu/lb } - ^\circ\text{F}$$

$$\rho_s = 0.321 \text{ lb/in}^3 = 554.7 \text{ lb/ft}^3$$

$$\text{PLANE SURFACE AREA, } A^*, = \frac{(102)(2)(2)(3.9375+3.1875)}{144} = 20.1875 \text{ ft}^2$$

HEAT TRANSFER AREA, A, = PLANE SURFACE AREA x SOLIDITY

$$A = A^*s$$

$$= (20.1875)(.8058)$$

$$A = 16.2667 \text{ ft}^2$$

FRONTAL AREA, A_{fr} , = 3.141" x 3.1875" = 10.012 in²

$$A_{fr} = 0.06953 \text{ ft}^2$$

It has been shown in Appendix A; however, that this can be alternately expressed as:

$$D_H = 4 \frac{P}{\beta}$$

Inasmuch as the perforations have no effect on the hydraulic diameter the value of β rather than $\bar{\beta}$ is used.

$$D_H = \frac{(4)(0.8834)}{(1742.1)} = \boxed{0.002028 \text{ ft}}$$

Now we are in a position to reduce the data. The following presentation outlines the steps required.

RECORDED DATA:

$d_o = 2.310''$	
$\Delta P_o = 6.69 \text{ in H}_2\text{O}$	$T_o = 69.9 \text{ }^\circ\text{F}$
$\Delta P_m = 10.15 \text{ in H}_2\text{O}$	$P_{\text{atm}} = 30.140 \text{ in Hg.}$
$P_s = 10.65 \text{ in H}_2\text{O}$	Chart Speed = 4 in/sec.
$P_o = 20.80 \text{ in H}_2\text{O}$	$\beta_o = d_o/d = \frac{2.310}{3.08} = 0.75$

DETERMINATION OF MASS RATE OF FLOW: (See Appendix A)

$$\dot{m} = \frac{589.81 F_a Y d_o^2 C}{\sqrt{1-\beta_o^4}} \Delta P_o \times \frac{P_3}{T_o}$$

where: $C = C_o + \Delta C \left[\frac{10^4}{N_R(d_o)} \right]$ from reference [13]

$$P_3 = (P_{\text{atm}} - P_o/13.6) 0.4912; T_o = t_o (^\circ\text{F}) + 459.7$$

$$Y = 1.0 \text{ Fig. 40b of Reference [14]}$$

$$F_a = 1.0 \text{ Fig. 30 of Reference [14]}$$

For $\beta_o = 0.75$ and $d = 3.08''$, $C_o = 0.60691$ and $\Delta C = 0.03839$, respectively.

$$P_3 = 30.140 - \frac{20.80}{13.6} \times 0.4912 = 14.0537 \text{ psi}$$

SOLID MATRIX CROSS SECTIONAL AREA, A_s ,

$$A_s = 102 \times 3.9375'' \times .0016'' + 103 \times 3.1875'' \times .0016''$$

$$= 1.1679 \text{ in}^2$$

$$A_s = 0.00811 \text{ ft}^2$$

FREE FLOW AREA, A_c , = FRONTAL AREA - SOLID CROSS SECTIONAL AREA

$$A_c = A_{fr} - A_s$$

$$A_c = 0.06142 \text{ ft}^2$$

CONDUCTION AREA CORRECTED FOR EFFECTS OF PERFORATIONS, A_k ,

$$A_k = A_s (1-\zeta) \text{ where } \zeta \text{ is the conduction area reduction ratio (See Appendix C).}$$

$$= 0.00811 (1-0.644)$$

$$A_k = 0.00288 \text{ ft}^2$$

POROSITY, p , = $\frac{\text{MATRIX FLOW VOID VOLUME}}{\text{MATRIX VOLUME}} = \frac{V_m - V_s}{V_m} = 1 - \frac{V_s}{V_m}$

$$p = 1 - \frac{0.00135}{0.01159} = 0.8834$$

COMPACTNESS, $\bar{\beta}$ = $\frac{\text{TOTAL HEAT TRANSFER AREA}}{\text{MATRIX VOLUME}}$

$$= \frac{A}{V_m} = \frac{16.2667}{0.01159} = 1403.75 \text{ ft}^2/\text{ft}^3$$

Note that $\bar{\beta}$ includes the effect of area reduction due to perforations.

β for an unperforated surface would therefore simply be the plane surface area divided by the matrix volume.

$$\beta = \frac{A^*}{V_m} = \frac{20.1875}{0.01159} = 1742.1 \text{ ft}^2/\text{ft}^3$$

THE HYDRAULIC DIAMETER, D_H , = $4r_h = \frac{4 \text{ FLOW CROSS SECTIONAL AREA}}{\text{WETTED PERIMETER}}$

$$T_o = 69.0 + 459.7 = 528.7 \text{ }^\circ\text{R}$$

$$\dot{m} = \frac{(589.81)(2.310)^2}{\sqrt{1 - (0.75)^4}} \times C \sqrt{6.69 \times \frac{14.0537}{528.7}}$$

$$\dot{m} = 1605.242 \text{ C}$$

assume $C = 0.6000$

then $\dot{m} = 963.145 \text{ lbm/hr}$

$$C = C_o + \Delta C \frac{10^4}{N_{R(d_o)}} \quad \text{where } N_{R(d_o)} = \frac{(4)(12)\dot{m}}{(3.1416)(3.08)\mu}$$

$$= 4.961 \frac{\dot{m}}{\mu}$$

μ is evaluated at temperature t_o by means of the linear approximation $\mu = 0.0395 + 0.64167 \times 10^{-4} t_o = 0.0395 + 0.64167 \times 10^{-4} (69.0)$
 $= 0.04392 \text{ lbm/hr ft}$

therefore,

$$C = 0.60691 + 0.03839 \frac{(10^4)(0.04392)}{(4.961)(963.145)}$$

$$C = 0.6104$$

This value of C is compared with the assumed value of C and successive iterations are performed until the two values are equal. The iterative process shows that a value of C = 0.6172 satisfies this requirement and thus

$$\dot{m} = 990.756 \text{ lbm/hr}$$

MATRIX REYNOLDS NUMBERS:

Two values for Reynolds number are required, one for the isothermal flow friction factor evaluation and second for the heat transfer evaluation. The two values differ only in so far as the difference in the absolute viscosities. μ_f is evaluated at orifice temperature (t_o) whereas μ_H (heat transfer) is evaluated at average bulk fluid temperature which is assumed to be at $t_o + 10^\circ\text{F}$.

$$N_{Rf} = \frac{4L\dot{m}}{A\mu_f} = \frac{(4)\frac{2}{12}(990.756)}{(16.2667)(.04392)} = \boxed{924.54}$$

$$N_{RH} = \frac{4L\dot{m}}{A\mu_H} = N_{Rf} \frac{\mu_f}{\mu_H} = 924.54 \frac{(.04392)}{(.04456)} = \boxed{911.23}$$

CONDUCTION PARAMETER:

$$\lambda = \frac{k A_k}{L \dot{m} c_p} = \frac{(38.7)(0.00288)}{(2/12)(990.756)(.24)} = 0.00282$$

$$\lambda_k = \lambda \frac{L}{L_k} \quad ; \quad \frac{L}{L_k} = 0.3351 \text{ from Appendix C.}$$

therefore

$$\lambda_k = (.00282)(.3351) = \boxed{0.000944}$$

MAXIMUM SLOPE:

The slope of the cooling curve was determined by the method prescribed in Appendix A from Figure 36. Slopes were determined for each of the curves and the average value was used.

$$\text{MAXIMUM SLOPE} = \frac{\bar{C}}{C} \left[\frac{dT}{d\theta} \right]_{\max} = \frac{\bar{C}}{C} \times \text{SLOPE} \times \text{CHART SPEED}$$

$$\bar{C}_s = W_s c_s = (0.68584 \text{ lb})(0.1065 \text{ Btu/lbm } ^\circ\text{F}) = 0.07304$$

$$C = \dot{m} c_p = (990.756 \text{ lb/hr})(0.24 \text{ Btu/lbm } ^\circ\text{F})(1 \text{ hr}/3600 \text{ sec}) = 0.06605.$$

$$\text{SLOPE} = 0.14357 \text{ (See Figure 36)}$$

whence,

$$\text{MAXIMUM SLOPE} = \frac{(.07304)}{(.06605)} (0.14357)(4) = \boxed{0.63507}$$

COLBURN j FACTOR:

Enter Table 1 or Figure 4 of Howard [5] or Figure 2-A of Howard [4] with the values of λ_k and MAXIMUM SLOPE to determine $N_{Tu} = 4.05$. Linear interpolation from this table is sufficient.

$$j = N_{Tu} \frac{A_c}{A} N_{PR}^{2/3} \text{ from Appendix A,}$$

$$N_{PR}^{2/3} = 0.8017 - 0.82353 \times 10^{-4} t_o \text{ using a linear approximation;}$$

therefore

$$j = (4.05) \frac{(0.06142)}{(16.2667)} (.7960) = \boxed{0.01217}$$

FANNING FRICTION FACTOR:

From Appendix A, the friction factor is:

$$f = \left[2g c_p \frac{\Delta P}{G^2} - (K_c - K_e) - \frac{\Delta P}{P_{\text{mean}}} (1+P^2) \right] \frac{r_H}{L}$$

$$P_{atm} = 30.140 \text{ in Hg} \times 0.4912 \frac{\text{psi}}{\text{in Hg}} = 14.8048 \text{ psi}$$

$$P_s = 10.65 \text{ in H}_2\text{O} \times 5.204 \frac{\text{psf}}{\text{in H}_2\text{O}} = 55.42 \text{ psf} = 0.3849 \text{ psi}$$

$$P_m = 10.15 \text{ in H}_2\text{O} \times 5.204 \frac{\text{psf}}{\text{in H}_2\text{O}} = 52.82 \text{ psf} = 0.3668 \text{ psi}$$

$$P_1 = P_{atm} - P_s = 14.8048 - 0.3849 = 14.4199 \text{ psi}$$

$$P_2 = P_1 - \Delta P_m = 14.4199 - 0.3668 = 14.0531 \text{ psi}$$

$$P_{mean} = \frac{P_1 + P_2}{2} = 14.2365 \text{ psi}$$

$$P_{mean} = \frac{P_{mean} (144)}{R(t_o + 459.7)} = \frac{(14.2365)(144)}{(53.35)(528.7)} = 0.07268 \text{ lbm/ft}^3$$

$$G = \frac{\dot{m}}{A_c} = \frac{990.756}{0.06142} = 16130.84 \text{ lbm/hr ft}^2 = 4.481 \text{ lbm/sec ft}^2$$

$$\frac{r_H}{L} = \frac{0.000507}{2/12} = 0.00304$$

$K_c = 0.48$ and $K_e = -0.33$ from Figure 5-3 of reference [8].

$$(1+p^2) = 1 + (0.8834)^2 = 1.7804$$

$$f = \left[\frac{(2)(32.2)(0.07268)(52.82)}{(4.481)^2} - (0.48 - 0.33) - \frac{.3668}{14.2365} (1.7804) \right] \times$$

$$(0.00304)$$

$$= (12.3126 - 0.150 - 0.04587)(0.00304)$$

$$f = 0.03686$$

The thermal properties, ν and $N_{PR}^{2/3}$, were obtained by linear interpolation of data from reference [3]. The values of k_s and c_s were obtained directly from references [2] and [1] for nickel and stainless steel respectively.

DOCUMENT CONTROL DATA - R&D		
<i>(Security classification of title, body of abstract and indexing annotation must be entered when the overall report is classified)</i>		
1. ORIGINATING ACTIVITY (Corporate author)		2a. REPORT SECURITY CLASSIFICATION
U. S. Naval Postgraduate School Monterey, California		unclassified
		2b. GROUP
		X
3. REPORT TITLE		
Heat Transfer and Flow Friction Characteristics of Perforated Nickel Plate-Fin Type Heat Transfer Surfaces.		
4. DESCRIPTIVE NOTES (Type of report and inclusive dates)		
Task Progress, January 1964 - June 1965.		
5. AUTHOR(S) (Last name, first name, initial)		
Bannon, J. M. Piersall, C. H., Jr. Pucci, P. F.		
6. REPORT DATE	7a. TOTAL NO. OF PAGES	7b. NO. OF REFS
30 June 1965	97	14
8a. CONTRACT OR GRANT NO.	9a. ORIGINATOR'S REPORT NUMBER(S)	
A. PROJECT NO.	TR - 52	
c.	9b. OTHER REPORT NO(S) (Any other numbers that may be assigned this report)	
d.		
10. AVAILABILITY/LIMITATION NOTICES		
"Qualified requesters may obtain copies of this report from DDC."		
11. SUPPLEMENTARY NOTES	12. SPONSORING MILITARY ACTIVITY	
	Bureau of Ships - Code 645	
13. ABSTRACT		
Experimental results for the convective heat transfer and flow friction characteristics of plate-fin type heat transfer surfaces are presented for eight surfaces. Six surfaces were fabricated of perforated nickel plate, one perforated nickel fins with solid nickel plate splitters and one of solid nickel plate. The heat transfer data were obtained by the transient technique and includes the effect of longitudinal conduction.		

14. KEY WORDS	LINK A		LINK B		LINK C	
	ROLE	WT	ROLE	WT	ROLE	WT
Heat Exchangers						
Heat Transfer Surfaces						
Regenerators						
Recuperators						

INSTRUCTIONS

1. ORIGINATING ACTIVITY: Enter the name and address of the contractor, subcontractor, grantee, Department of Defense activity or other organization (*corporate author*) issuing the report.

2a. REPORT SECURITY CLASSIFICATION: Enter the overall security classification of the report. Indicate whether "Restricted Data" is included. Marking is to be in accordance with appropriate security regulations.

2b. GROUP: Automatic downgrading is specified in DoD Directive 5200.10 and Armed Forces Industrial Manual. Enter the group number. Also, when applicable, show that optional markings have been used for Group 3 and Group 4 as authorized.

3. REPORT TITLE: Enter the complete report title in all capital letters. Titles in all cases should be unclassified. If a meaningful title cannot be selected without classification, show title classification in all capitals in parenthesis immediately following the title.

4. DESCRIPTIVE NOTES: If appropriate, enter the type of report, e.g., interim, progress, summary, annual, or final. Give the inclusive dates when a specific reporting period is covered.

5. AUTHOR(S): Enter the name(s) of author(s) as shown on or in the report. Enter last name, first name, middle initial. If military, show rank and branch of service. The name of the principal author is an absolute minimum requirement.

6. REPORT DATE: Enter the date of the report as day, month, year, or month, year. If more than one date appears on the report, use date of publication.

7a. TOTAL NUMBER OF PAGES: The total page count should follow normal pagination procedures, i.e., enter the number of pages containing information.

7b. NUMBER OF REFERENCES: Enter the total number of references cited in the report.

8a. CONTRACT OR GRANT NUMBER: If appropriate, enter the applicable number of the contract or grant under which the report was written.

8b, 8c, & 8d. PROJECT NUMBER: Enter the appropriate military department identification, such as project number, subproject number, system numbers, task number, etc.

9a. ORIGINATOR'S REPORT NUMBER(S): Enter the official report number by which the document will be identified and controlled by the originating activity. This number must be unique to this report.

9b. OTHER REPORT NUMBER(S): If the report has been assigned any other report numbers (*either by the originator or by the sponsor*), also enter this number(s).

10. AVAILABILITY/LIMITATION NOTICES: Enter any limitations on further dissemination of the report, other than those

imposed by security classification, using standard statements such as:

- (1) "Qualified requesters may obtain copies of this report from DDC."
- (2) "Foreign announcement and dissemination of this report by DDC is not authorized."
- (3) "U. S. Government agencies may obtain copies of this report directly from DDC. Other qualified DDC users shall request through _____."
- (4) "U. S. military agencies may obtain copies of this report directly from DDC. Other qualified users shall request through _____."
- (5) "All distribution of this report is controlled. Qualified DDC users shall request through _____."

If the report has been furnished to the Office of Technical Services, Department of Commerce, for sale to the public, indicate this fact and enter the price, if known.

11. SUPPLEMENTARY NOTES: Use for additional explanatory notes.

12. SPONSORING MILITARY ACTIVITY: Enter the name of the departmental project office or laboratory sponsoring (*paying for*) the research and development. Include address.

13. ABSTRACT: Enter an abstract giving a brief and factual summary of the document indicative of the report, even though it may also appear elsewhere in the body of the technical report. If additional space is required, a continuation sheet shall be attached.

It is highly desirable that the abstract of classified reports be unclassified. Each paragraph of the abstract shall end with an indication of the military security classification of the information in the paragraph, represented as (TS), (S), (C), or (U).

There is no limitation on the length of the abstract. However, the suggested length is from 150 to 225 words.

14. KEY WORDS: Key words are technically meaningful terms or short phrases that characterize a report and may be used as index entries for cataloging the report. Key words must be selected so that no security classification is required. Identifiers, such as equipment model designation, trade name, military project code name, geographic location, may be used as key words but will be followed by an indication of technical content. The assignment of links, roles, and weights is optional.